A MECHANISTIC VIEW OF CULLIN NEDDYLATION: ALLOSTERIC CONFORMATIONAL CONTROL OF E3-RING LIGASES

by

Melis Yıldırım

B.S., Chemical Engineering, Boğaziçi University, 2012

Submitted to the Institute for Graduate Studies in
Science and Engineering in partial fulfillment of
the requirements for the degree of
Master of Science

Graduate Program in Chemical Engineering

Boğaziçi University

2014

ACKNOWLEDGEMENTS

First and foremost, I would like to express my sincere gratitude to my thesis advisor, Professor Türkan Haliloğlu for her perpetual guidance, motivation and support throughout my studies. She is the one who has initiated my enthusiasm and passion towards conducting research. I owe my deepest appreciation to her for the invaluable education that she has gained to me.

I would like to thank my committee members; Professor Pemra Doruker Turgut and Assistant Professor Pemra Özbek for their constructive criticisms and valuable recommendations to my research. Additionally I would like to express my deep gratitude to Professor Ruth Nussinov for her motivation and counsel. Her advices will always shed a light on my future profession.

It is a pleasure for me to thank Fidan Sümbül for her valuable advices, criticisms on my research and endless patience for my frequent questions. She has turned my late at night studies in Polymer Research Center to joy with her presence. Also I would like thank specifically to Arzu Uyar for her endless care and support. Without her support, it would be much difficult to complete this thesis. My deepest appreciations are for the PRC members: Burçin Acar, Zeynep Kürkçüoğlu Soner, Seren Soner, Burcu Aykaç Fas, Serdar Özsezen, Zeynep Erge Akbaş, Cihan Kaya, Nurver Tezcan, Gökçe Ezeroğlu, Canan Dedeoğlu and Yüksel Gülten; and my dearest friends Can Ekici, Serhat Erşahin, Özgür Yaşar Çağlar, Gülce Güldür, Dilruba İnam, Mustafa Türkekul, Emine Güven-Maiorov, Serena Muratçıoğlu, Tuğçe Erbay and İrem Şen.

Finally, my special thanks are for my family; my mother for her motivation, my father for his support, my sisters Nil and Sera for making me smile, my grandmothers for their care, Esra-Metin Canbaz and Selma-Orhan Önel for their trust in me, and of course my fiancé Onur Önel for always being by my side with his love. I dedicate this thesis to them.

ABSTRACT

A MECHANISTIC VIEW OF CULLIN NEDDYLATION: ALLOSTERIC CONFORMATIONAL CONTROL OF E3-RING LIGASES

Cullin-RING E3 ligases (CRLs), which constitute a superfamily of RING type E3 ligases, regulate ~20% of protein degradation by the ubiquitin-proteasome system in the cells. Cullin neddylation activates CRLs by urging a conformational transition in Cullin C-terminal domain and exposes the Rbx1 RING E3 ligase to facilitate ubiquitination. CRLs are over-activated by Cullin neddylation in myriad of human cancers; thereby the inhibition mechanism of Cullin neddylation is of significant interest for generating novel cancer therapies. To explore how the signals of Cullin neddylation are transmitted through the CRLs to control the Rbx1 conformations, we performed molecular dynamics (MD) simulations combined with Gaussian Network Model (GNM) analysis on the closed-unbound and open-bound to Nedd8 states of Cul5-Rbx1 E3 ligases. Our results display multiple Rbx1 RING domain conformations with neddylation of Cul5 where the rigid dynamics of the unbound-to-Nedd8 state CRLs is abrogated. The Rbx1 RING domain conformations of the neddylated CRLs, which are in agreement with the proposed neddylated state Rbx1 conformations for effective ubiquitin transfer, arise as a result of coupled dynamics between Nedd8 and Rbx1. A dynamic hinge plane of Cul5 hinges at R495-M496, N704-E705 and Rbx1 hinges at D51-L52, T69-V70 coordinates allosteric communication between Nedd8 and Rbx1 on the CRL structure along an H-bond between Cul5 R538, R569 and Rbx1 E67 that restricts the Rbx1 conformational space. Nedd8 predisposes Rbx1 together with Cul5 for an effective ubiquitin transfer by a plausible mechanism explaining the allosteric conformational control of Rbx1. We propose that selective interruptions in the neddylation pathway to disrupt the dynamic hinge plane coordination could shed a light on the allosteric drug design studies on Cullin neddylation inhibition.

ÖZET

CULLIN NEDİLASYONU ÜZERİNE MEKANİSTİK BİR BAKIŞ AÇISI: E3-RING LİGAZLARININ ALOSTERİK KONFORMASYONEL KONTROLÜ

Ubikuitin-proteazom sistemi tarafından gerçekleştirilen protein degradasyon işlemlerin yaklaşık %20'si E3-RING ligazlarının bir alt familyasına ait olan Cullin-RING E3 ligazları (CRL) aracılığıyla gerçekleşmektedir. Nedd8 proteinin Cullin proteinlerine bağlanması sonucu gerçekleşen Cullin nedilasyonu Cullin karboksi terminal bölgelerinde ve bu bölgeye bağlı E3-RING ligazların RING bölgelerinde önemli konformasyonel değişikliklere yol açar ve böylece CRL proteinlerini etkinleştirir; hücreyi daha hızlı ve verimli bir ubikuitinasyon sürecine sokar. Son yıllarda yapılan çalışmalar kanserli hücrelerin bir çoğunda CRL proteinlerinin Cullin nedilasyonu sonucu beklenilenin üzerinde etkinleştirildiği görülmüştür. Dolayısıyla son yıllarda yürütülen anti-kanser tedavi araştırmaları Cullin nedilasyonunun imha edilmesi üzerine yoğunlaşmıştır. Nedd8 proteininin E3-RING ligazlarının konformasyonlarını nasıl kontrol ettiğini araştırmak amacıyla Culin5-Rbx1 E3 ligazlarının nedilasyondan önceki ve sonraki yapıları Moleküler Dinamik (MD) simulasyonları ve Gaussian Ağyapı Model analizleri ile incelenmiştir. Sonuçlar Cullin nedilasyonu ile birlikte CRLlerdeki sabit yapı dinamiğinin terkedildiğini ve E3-RING ligazı olan Rbx1'ın birden fazla sayıda konformasyona büründüğünü ortaya koymuştur. Elde edilen Rbx1 konformasyonlarının önceki çalışmalarda öne sürülen RING konformasyonlarıyla uyum içinde olduğu görülmüş ve bu konformasyonların Nedd8 ile Rbx1 arasındaki anlaşmalı dinamiği sonucu ortaya çıktığı bulunmuştur. Eklem özelliği gösteren Cullin5 R495-M496, N704-E705 ve Rbx1 D51-L52, T69-V70 amino asitlerinin oluşturduğu bir dinamik bir düzlem ile birlikte Cullin5 R538, R569 ve Rbx1 E67 amino asitleri arasındaki hidrojen bağı aracılığıyla Rbx1 konformasyonel alanının kısıtlandığı ve böylece Nedd8-Rbx1 arasındaki alosterik etkileşimin koordine edildiği görülmüştür. Nedd8, Cullin5 proteini yardımıyla Rbx1 konformasyonunu verimli bir ubikuitinasyon işlemi için yatkın hale getirmektedir. CRLlerde önerilen dinamik düzlem koordinasyonuna engel olacak şekilde Cullin nedilasyon metabolik yolunda müdahalelerde bulunulması Cullin nedilasyonunu inhibe edecek alosterik ilaç tasarımı çalışmalarına yardımcı olabilir.

TABLE OF CONTENTS

LIST OF FIGURES

LIST OF TABLES

LIST OF SYMBOLS

a_i	Acceleration of the particle i
$C\alpha$	Alpha Carbon
C_{ij}	Cross-correlations between residue i and j
dt	Time step
dr_i	Positional derivative
F	Force exerted on the particle
k_B	Boltzmann constant
kDa	Atomic mass unit, kiloDalton
m	Mass of the particle
N	Number of atoms
ns	Nanoseconds
ps	Picoseconds
r_{cut}	Cutoff radius
$\boldsymbol{r}_i$	Position vector of particle i
$\boldsymbol{r}_i^0$	Initial position vector of particle i
$\Delta\boldsymbol{r}_i$	Change in position vector of particle i
t	Time
T	Temperature in Kelvin
$\boldsymbol{U}$	Eigenvector matrix obtained by Kirchoff matrix decomposition
U_i	Potential energy function of the particle i

u_k	Eigenvector of the kth mode
v_i	Velocity of the particle i
α	Alpha
Å	Angstrom
β	Beta
γ	Force constant
Γ	Kirchoff connectivity matrix
λ_k	Eigenvalue of the kth mode
$\boldsymbol{\Lambda}$	Eigenvalue matrix obtained by Kirchoff matrix decomposition

LIST OF ACRONYMS/ABBREVIATIONS

4HB	4-helix bundle
A	Alanine
C	Cysteine
CAND1	Cullin-associated NEDD8-dissociated protein 1
CHARMM	Chemistry at HARvard Macromolecular Mechanics
CRL	Cullin-RING E3 ligase
CSN	Cop9 signalosome
CTD	C-terminal domain
D	Aspartic acid
DEN1	Dengue virus type 1
DNA	Deoxyribonucleic acid
E	Glutamic acid
ENM	Elastic Network Model
F	Phenylalanine
G	Glycine
GNM	Gaussian Network Model
H	Histidine
I	Isoleucine
K	Lysine
L	Leucine
M	Methionine

MD	Molecular dynamics
MMTSB	Multi-scale Modeling Tools for Structural Biology
MSF	Mean square fluctuations
MOE	Molecular Operating Environment
N	Asparagine
NAE	Nedd8 activating enzyme
NAMD	Nano-scale Molecular Dynamics
NEDD8	Neural Precursor cell expressed, developmentally down-regulated gene 8
NMA	Normal Mode Analysis
NTD	N-terminal domain
P	Proline
PCA	Principal Component Analysis
PDB	Protein Data Bank
Q	Glutamine
R	Arginine
Rbx	RING Box
RING	Really Interesting New Gene
RMSD	Root mean square deviation
S	Serine
SCF	SKP1-Cullin-Fbox
SKP1	S-phase kinase-associated protein 1
T	Threonine
UBC	Ubiquitin-Conjugating Enzyme

UBL	Ubiquitin-like protein
UPS	Ubiquitin-Proteasome System
W	Tryptophan
WHB	Winged-helix beta
V	Valine
VMD	Visual molecular dynamics
Y	Tyrosine

1. INTRODUCTION

Dynamic equilibrium is significant in every terms of life, beginning in the most basic units of living organisms, cells. Most of the cellular processes including cell cycle and regulation of gene expression require an appropriate balance in intracellular protein levels to protect cellular homeostasis. The guard of the cellular homeostasis is the ubiquitination which is the process of tagging the targeted regulatory proteins with ubiquitin to degrade them [1-4]. Tagging proteins with ubiquitin does not solely controls protein degradation but also affects protein sorting, enzymatic activity and protein-protein interactions [5].

Ubiquitin is an evolutionary conserved 76 amino acid polypeptide which covalently attaches to the proteins needed to be destroyed [5, 6]. Sequential enzymatic cascade is involved in the ubiquitin conjugation to the target proteins. First, a covalent bond between the ubiquitin activating enzyme (E1) and ubiquitin is formed which is followed by ubiquitin transfer from E1 to ubiquitin-conjugating enzyme (E2) and then ubiquitin transfer from E2 to a substrate protein which is recruited by E3 ubiquitin ligases. The final step is the degradation of polyubiquitin-labeled substrates by the 26S proteasome [5, 7]. The RING (Really Interesting New Gene) E3 ligases are largest known subclass of E3 ubiquitin ligases [4, 8]. E3-RING ubiquitin ligases ramify into two protein families; Rbx1 and Rbx2. E3-RING ubiquitin ligases co-operate with the Cullin proteins and form the multi-subunit Cullin-RING ubiquitin ligases (CRLs) [9].

Proteins associated with cell cycle regulation, cell growth and proliferation, intracellular signaling, DNA repair, membrane-receptor regulation, pro and anti-apoptotic signaling consist the substrates of CRL mechanisms in the ubiquitin-proteasome system (UPS) [10]. Loss of specific function in the ubiquitination pathway or any dysregulation in the UPS can result in uncontrolled cell proliferation, inappropriate loss of regulatory proteins or sustained activation of specific signal cascade which potentially cause cancer or other neurodegenerative disease developments [11-13]. Therefore modulating the ubiquitination pathway is a potential therapeutic anticancer treatment.

In recent years, allosteric effectors on the ubiquitination pathway have been well-studied as potential therapeutic drugs [14]. Allostery is an essential concept for understanding the intramolecular control, that includes the effect of perturbation on a protein site by a ligand binding or a chemical modification on a distal site of the protein [15]. To understand the protein activities in the multi-subunit complex structures, including the CRLs, allostery is reported as an inevitable process [16].

On the other hand ubiquitination is not the unique process that regulates the protein degradation mechanism. Covalent attachment of ubiquitin-like proteins to the target substrates also regulates the cellular apoptosis [12]. Nedd8 is one of those ubiquitin-like proteins whose conjugation to the targets are called neddylation [17]. Neddylation conjugation pathway has a major role in interceding protein ubiquitination and numerous biological regulations within the cells. Cullins are the most favored qualified substrate proteins of Nedd8 [18]. Neddylation of Cullins stimulates the CRL activity [18, 19], which lead Cullin C-terminal domain (CTD) to a significant conformational re-arrangement [20].

In human cancers, CRLs are overactivated by the overexpression of Nedd8. Thereby, in recent years, in addition to the inhibition of ubiquitination pathway by bortezomib, a novel therapeutic approach for anticancer therapy has come into the stage, Cullin neddylation pathway inhibition [12, 18, 21-23] Despite of the certain cancer cell selectivity attained by reversible inhibition of 26S proteasome by bortezomib, cytotoxicity is reported as a major problem for the ubiquitination-pathway inhibition type of therapeutic approach [12, 24]. Whereas selective interruption in the neddylation conjugation pathway may be a promising approach which could be less involved in toxicity [11].

According to the World Cancer Report 2014, cancer diagnoses have been forecasted to increase by about 70% worldwide in two decades. Therefore, it is essential to understand the structural dynamics of neddylated Cullins for further development of the novel anticancer therapeutic approach, neddylation pathway inhibition. At the present time, Protein Data Bank has $Cul5^{CTD}$-Rbx1 E3 ubiquitin ligase crystal structures both in neddylated and unneddylated states [20]. Hence, in this thesis, structural dynamics of the $Cul5^{CTD}$-Rbx1 E3 ubiquitin ligase, before and after neddylation, and also after deneddylation are investigated through Molecular Dynamic (MD) simulations in comply

with the Gaussian Network Model. The conformational and dynamics alterations within the $Cul5^{CTD}$-Rbx1 E3 ubiquitin ligases upon Nedd8 conjugation are studied and the allosteric interactions within the neddylated CRL mechanism are derived to acquire beneficial information for the future effective cancer treatment studies.

2. LITERATURE SURVEY

2.1. Ubiquitin and Its Functions

Ubiquitin was first identified by Edward A. Boyse and his research group in 1975. It was introduced as a 8.5 kDa protein of unknown function expressed and conserved in all eukaryotic cells [25]. Originally, ubiquitin was named as ubiquitous immunopoietic polypeptide (UBIP). In 1980s, the basic functions and the pathway of ubiquitination were enlightened by Aaron Ciechanover, Avram Hershko and Irwin Rose. The Nobel Prize in Chemistry 2004 was awarded jointly to them for the discovery of ubiquitin-mediated protein degradation [26].

Ubiquitin is a small highly conserved protein which is "ubiquitously" found in all eukaryotic cells. Covalently attachment of this protein to the target substrate proteins' lysine residues via its carboxyl-terminal glycine residue and thus formation of an iso-peptide linkage between them is called ubiquitination process [27]. The substrate proteins which have ubiquitin chain on their Lysine 48 (K48) linkage are identified by 26S proteasomes for targeted degradation. On the other hand, substrates having ubiquitin chain on their Lysine 63 (K63) linkage can be activated to regulate the NF-κB signaling pathway [28, 29], DNA replication and repair [30, 31], and intracellular trafficking [32] (Figure 2.1).

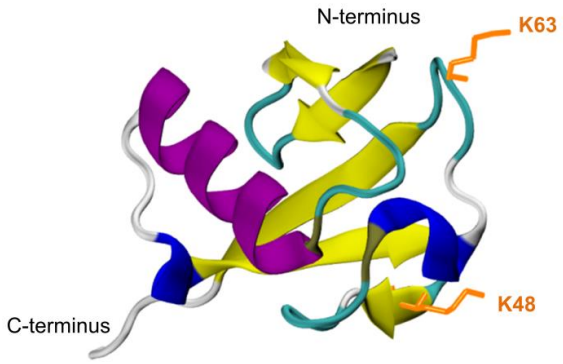

Figure 2.1. Structure of Ubiquitin – PDB Code: 1UBQ. Structure is colored according to its secondary structure. Significant LYS side chains are shown in orange sticks.

2.2. Ubiquitination and Neddylation Pathways

Ubiquitination modulates the cell physiology with not only ubiquitin, but also several different "ubiquitin-like" proteins such as SUMO and Nedd8. Nedd8 is an 81-amino acid protein with 9 kDa relative molecular mass which shares approximately 60% sequence identity and 80% homology with ubiquitin [12, 33]. Nedd8 was discovered by Kumar *et al.* in 1992 as one of the ten mouse neural precursor cell-expressed, developmentally down-regulated (NEDD) genes [34]. Just like ubiquitin, Nedd8 is attached to its substrates via an isopeptide linkage between its carboxyl-terminal glycine 76 and a lysine of the target protein [17]. This covalent attachment of Nedd8 to the substrates is called neddylation. The most popular substrates of Nedd8 are the Cullin proteins and Nedd8 conjugation onto Cullins is referred as Cullin neddylation.

Ubiquitination occur via three enzyme cascade within the cells, ubiquitin-activating enzyme (E1), ubiquitin-conjugating enzyme (E2) and ubiquitin ligases (E3) [1, 2, 4, 6, 12, 35]. Activation of the ubiquitin by E1 in an ATP-dependent manner is the initial point of the ubiquitination pathway [36, 37]. Although, ubiquitin-activating enzyme E1 was thought as the unique E1 type enzyme responsible for ubiquitin activation since its discovery, recent studies of Hofmann and his group identified a relatively uncharacterized E1 enzyme, designated ubiquitin-like modifier activating enzyme 6 (UBA6) which also activates ubiquitin [38].The E1 enzyme transfers the activated ubiquitin to the cysteine residue of E2 enzyme. To date 38 E2 enzymes have been identified in human and the number is continuing to increase. The increase of E2s relative to the known E1s is explained with the substrate specificity. Due to the distinct primary sequences in the core domains of E2s, they can specify cognate E3s in addition to the substrate specify and localization [5, 39] . Final step in this sequential enzymatic cascade is the ubiquitin transfer from E2 enzyme to E3 ligase which facilitates the ubiquitination of substrate protein. Similar pathway is valid for neddylation. Neddylation is initiated by an E1 enzyme specific to Nedd8 (Nedd8-activating enzyme: NAE) which forms Nedd8 adenylate by utilizing ATP. Nedd8 is then transferred to a specific cysteine residue within NAE. With the trans-thiolation reaction, Nedd8 is transferred from Nedd8-NAE thioster to specific E2 enzymes for Nedd8 (Ubc12 or UBE2F) and finally Nedd8 is delivered to cognate E3 ligases of

specific E2 enzymes. The neddylation process can facilitate the E3-catalyzed ubiquitination and consequently substrate ubiquitination [11, 20] (Figure 2.2).

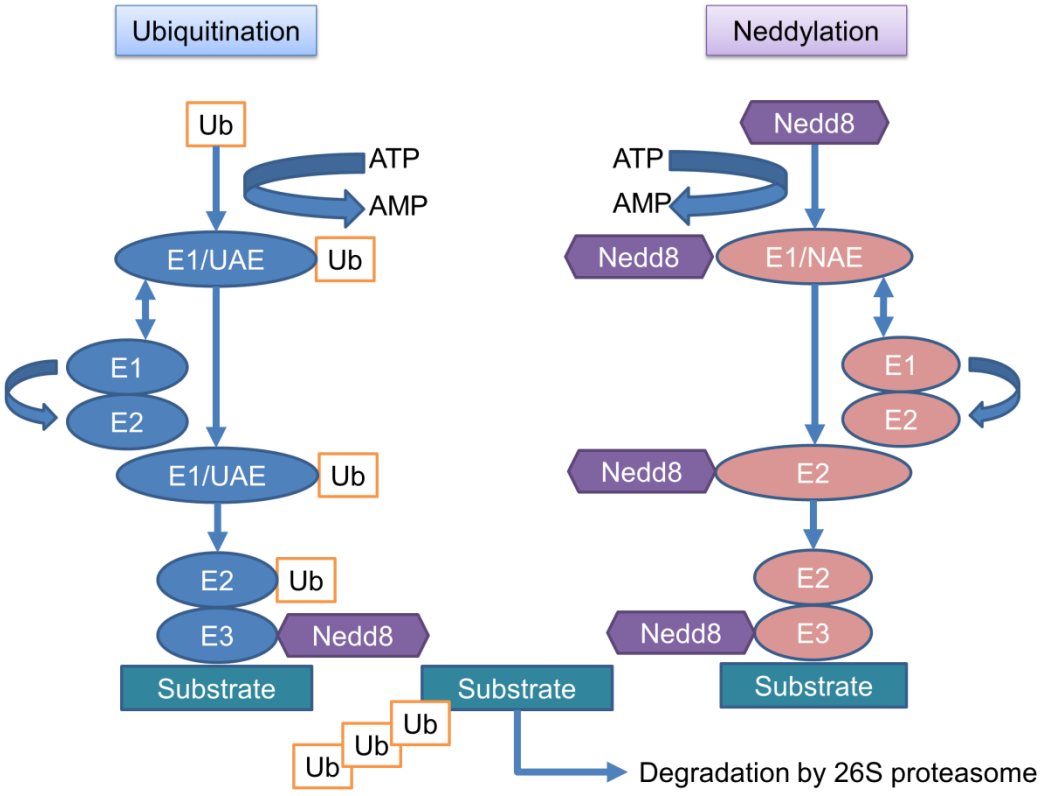

Figure 2.2. Schematic representation of ubiquitination and neddylation pathways.

2.3. The Roles of COP9, DEN1 and CAND1 in Cullin Neddylation Pathway

Neddylation is a reversible process [21]. Deneddylation of CRLs is regulated by COP9 signalosome (or CSN), a protein complex comprising 8 subunits [40]. In addition to COP9, DEN1 also mediates the Cullin deneddylation in vitro. However; in vivo COP9 is the responsible for Cullin deneddylation whereas DEN1 regulates deneddylation of other proteins, thus their activates are not overlapping [41]. After deneddylation of CRLs, CAND1 binds to deneddylated CRL complexes in order to block the binding sites of adaptor proteins and Nedd8. This blocking keeps the CRLs in a rigid-off state and prevents the assembly with substrate receptor proteins and dynamic activation by Cullin modification by Nedd8. Nevertheless CAND1 is required together with COP9 for efficient CRL activity [42, 43].

2.4. Cullin-RING Ligases: The Largest Subclass of E3 Ubiquitin Ligases

Thus far, several hundreds of E3s showing substrate specificity have been discovered in the ubiquitination pathway which are ramified into three distinct classes based on their domain found in their core proteins: HECT (homologues to E6-AP carboxy terminus), RING (really interesting new gene) and U-box E3 ligases [44].

Among the E3 ligases, Cullin-RING E3 ligases (CRLs), which are also known as SKP1-Cullin-Fbox (SCF) E3 ligases, is the largest known multi-unit ubiquitin ligases [4, 42]. About 20% of the UPS-regulated proteins' ubiquitination and degradation are controlled by CRLs [12, 45]. CRLs consist of a Cullin scaffold protein together with a catalytic RING (Really Interesting New Gene) subunit which binds to Cullin C-terminal domain, specifically Rbx1 and Rbx2 [12, 46]. The human genome encodes six Cullin proteins: Cul1, Cul2, Cul3, Cul4A/Cul4B, Cul5 and Cul7 [4, 19, 45]. Together with the adaptor proteins bound to Cullin N-terminal domain and substrate receptor protein bound to the adaptor protein, Cullin and Rbx1/2 proteins constitute various subfamilies of CRL mechanisms [42, 47] (Figure 2.3).

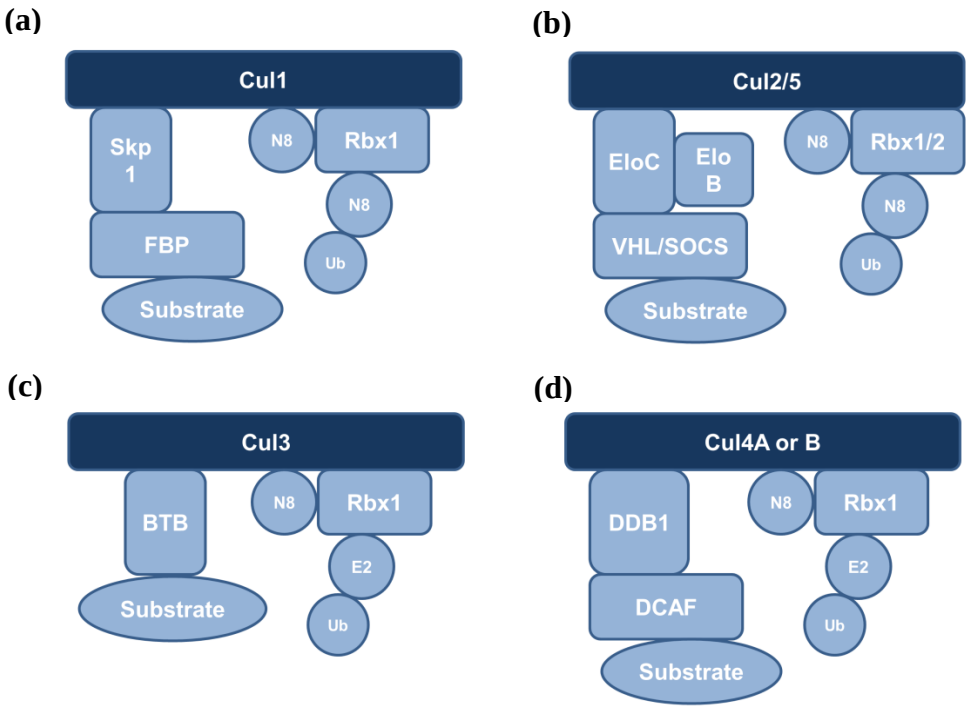

Figure 2.3. Cullin RING E3 Ligase Complexes.

2.5. Nedd8 Conjugation to Cullins: Scaffold Proteins of Cullin-RING Ligases

Nedd8 has been shown to regulate all types of Cullins by covalent attachment to them. Figure 2.4 presents the ubiquitination (Figure 2.4a) and Cullin neddylation (Figure 2.4b) mechanism. In Figure 2.4, S stands for substrate which is aimed to be ubiquitinated. Substrate binding proteins, located on the left arm of the Cullin proteins, have two domains: substrate binding domain (SBD) and the Box domain. Cullins also have two domains: C and N-terminal domains, CTD and NTD respectively. Cul^{CTD} ramifies into 3 subdomains: 4HB, α/β and WHB domains. Besides, RING E3 ligases, which are Rbx proteins, have two domains. The functionally significant residues for ubiquitination and Cullin neddylation are printed. Cullin lysine residue where Nedd8 conjugates is represented with K on Cul CTD WHB domain and C represents the cysteine residue on E2 where ubiquitin and Nedd8 ensconced on for ubiquitination and neddylation respectively. The Cullin neddylations highly facilitate the CRL-dependent ubiquitination [12].

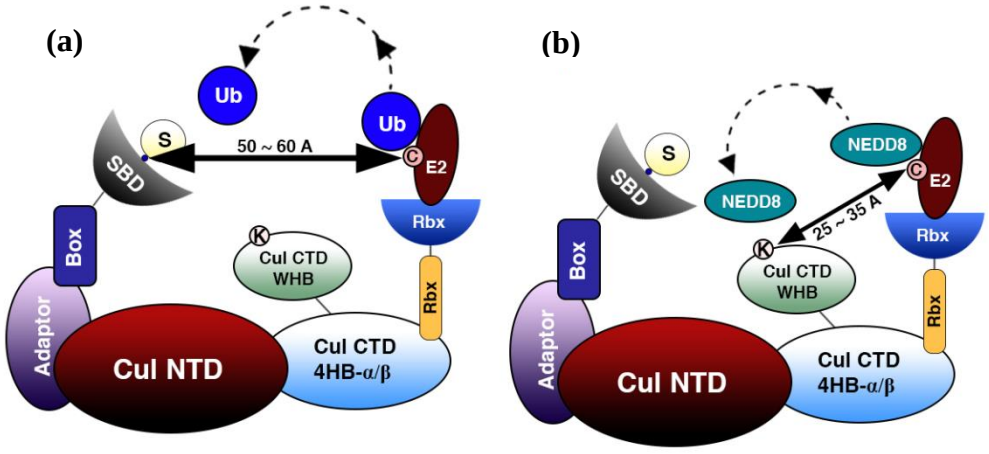

Figure 2.4. Ubiquitination (a) and Cullin neddylation (b) in CRLs.

In 2008, among over 100 different neddylated CRL complexes of Cul1-5 and Rbx1-Rbx2 from numerous species, only one high diffraction-quality crystals of a neddylated CRL from human was acquired by Duda *et al.*, which is Nedd8 conjugated $Cul5^{CTD}$-Rbx1 complex [20]. A striking conformational rearrangement has been presented in the crystal structure of neddylated $Cul5^{CTD}$-Rbx1 complex which highly promotes substrate ubiquitination. Nedd8 conjugation to Cul5 induces major conformational changes in the Cul5 C-terminal domain (CTD) which not only eliminates a binding site for the CRL

inhibitor CAND1 but also relocates the E2-binding RING domain of Rbx1 from the Cul5. Neddylation of Cul5 frees the Rbx1 linker from its binding pocket on the Cul5^{CTD} and thus Rbx1 becomes flexibly linked to the scaffold Cullin structure. The Figure 2.5 presents the change in CRL mechanism upon Cullin neddylation. In Figure 2.5, Rbx1 is represented by R and Nedd8 with N. The Cullin CTD is emphasized with a dashed box where Nedd8 attaches on Cullin protein. The neddylated CRL structure can be visualized with a balloon-like protein (Rbx1 in this work) that is tied to a rigid body object (Cul5^{CTD} in this work) and flies freely. Due to the flexible nature of the Rbx1, the gap between the ubiquitin and the substrate protein is potentially closed and subsequently substrate becomes ubiquitinated [48].

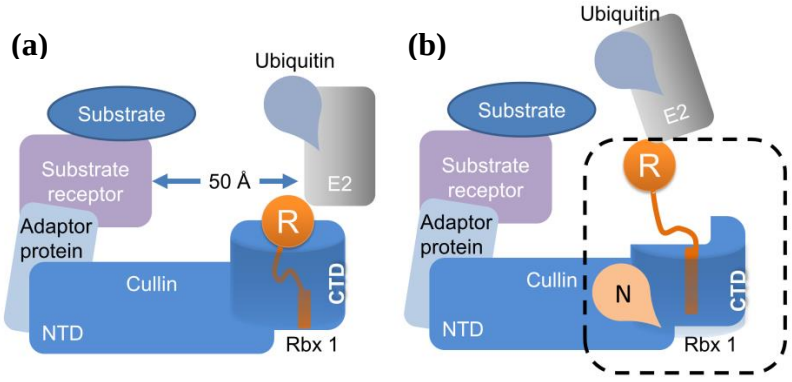

Figure 2.5. Unmodified (a) and neddylated (b) forms of CRL mechanisms.

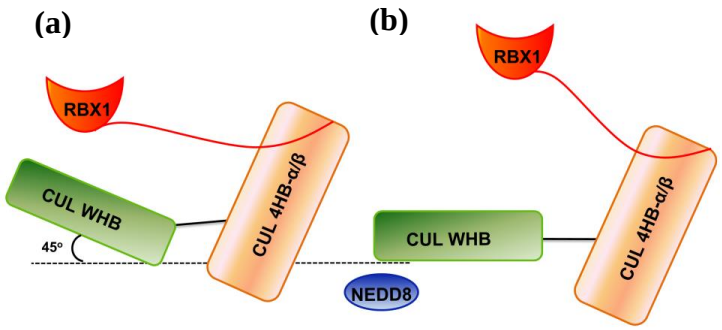

Figure 2.6. Schematic representation of the unmodified (a) and neddylated (b) CRLs.

The crystal structures of Cul5^{CTD}-Rbx1 complex either in closed conformation, which is the wild state without any Nedd8 perturbation (3DPL), and open conformation, which is Nedd8 conjugated Cul5^{CTD}-Rbx1 complex (3DQV) have been identified by Duda *et al.* [20]. The schematic representation of the CRL complex domains are shown in the Figure 2.6 in both the unmodified and neddylated CRL conformations.

2.6. Recent Studies on Cullin5 E3-RING Ligases

The substrate binding proteins of Cullin 5 E3 ligases are belong to the suppressor of cytokine signaling (SOCS) family which consists of 8 members (SOCS1-7, CIS). SOCS comprises N-terminal domain, a SH2 domain and a C-terminal domain SOCS box which is also subdivided into two regions; a BC box responsible for binding Elongin BC (specific adaptor proteins of Cul5) and a Cul5 box which provides the direct interaction with Cul5 [45, 47].

In 2005, the presence of SOCS1 biallelic mutation is shown in mediastinal lymphoma and also it has been found that ectopic expression of SOCS1 downregulates JAK2-STAT5 signaling [49]. Also the promoter of SOCS3 promoter has been displayed to be hypermethylated in lung cancer cell lines and primary tumor specimens resulting in reduced SOCS3 protein expression and elevated pSTAT3 expression [50].

Furthermore, human adenovirus serotype 5 (Ad5) products, E4orf6 and E1B55k, interact with Cul5 E3 ligases to organize p53 degradation which requires an intact Nedd8 pathway [51]. Similar mechanism to promote tumor suppressors VHL and p53 degradation was found to be utilized by Kaposi's sarcome-associated herpes virus (KSHV)-encoded latency-associated nuclear antigen (LANA) in collaboration with Cul5 E3 ligases [52]. Besides, in 2009, a link between Cul5 E3 ligase and the heat shock protein 90 (HSP90) chaperone complex, which participates in the folding of its client protein into their functional conformation, was reported [53]. Among HSP90 clients, numerous of them are identified in several cancer types.

On the other hand, conjugation of Nedd8 to Cul5 by the Nedd8-conjugating enzyme UBE2F is found to be necessary for HIV Vif-mediated degradation of the host restriction factor APOBEC3G (A3G) [18, 54]. Inhibiting Vif in order to protect the A3G family activities requires the inhibition of neddylation of Cul5 [18, 54].

Moreover, various computational studies have been performed to investigate the structural dynamic behavior of Cul5-Rbx1 mechanism during ubiquitination. In order to explore the dynamics of substrate binding proteins of several Cullin-RING E3 ligases in positioning and orienting the substrates for ubiquitin transfer, several substrate binding

proteins such as VHL-box, SOCS-box and F-box proteins were simulated in the unbound form and bound to their cognate adaptor proteins; in which Cullin 5 E3 ligase's substrate binding proteins, SOCS2 and SOCS4, were also included. The results show that the flexible inter-domain linker in SOCS2 and SOC4 serves as a hinge which rotates the substrates binding domain and positions it in an optimum manner for ubiquitin transfer [55].

In 2010, conformational changes in the C-terminal domain of Cul5 due to Nedd8 conjugation are studied via MD simulations by Liu *et al.* [46]. Before neddylation, the linker flexibility of Rbx1 has been found to lead to conformational changes in the CRL mechanism which permits neddylation and initiation of ubiquitination. Additionally, it is reported that the large Nedd8 induced conformational changes in the Cullin 5 C-terminal domain were retained after deneddylation which allows both initiation of ubiquitination and ubiquitin chain elongation after deneddylation. Finally, a mutation in the lysine residue where Nedd8 binds to Cul5 was found to cause a significant decrease in CRL conformational changes which reflects the allosteric regulation of CRLs by the acceptor lysine.

Another interest was the probability of any allosteric regulation in the CRL mechanisms. In addition to the substrate binding proteins and Rbx proteins of CRL mechanisms, the role of Cullins in the CRL complexes was tried to be enlightened via simulating Cul1, Cul4A and Cul5 crystal structures [56]. Allosteric functional roles of Cullins in the CRL mechanisms were inquired and the results showed that Cullins do not display intrinsic rigid scaffold characteristics, but are flexible with conserved hinges in the Cullin N-terminal domain. Cullins are further reported to allosterically regulate ubiquitination by means of this flexible nature.

2.7. Cullin Neddylation Inhibition as a Novel Anticancer Therapy Approach

The protein turnover within the cells is regulated by the ubiquitin-proteasome system (UPS). UPS regulates the protein degradation [5]. Proteins associated with cell cycle regulation, cell growth and proliferation, intracellular signalling, DNA repair, membrane-receptor regulation, pro and anti-apoptotic signalling consist the substrates of

CRL mechanisms in the ubiquitin-proteasome system (UPS) [10]. Any dysregulation in the UPS or loss of specific function in the ubiquitination pathway may result in the sustained activation of signaling pathways, uncontrolled cell proliferation and/or inappropriate loss of regulatory proteins and thus cancer and neurodegenerative disease developments [12].

Studies have revealed that the ubiquitination pathway modification is a potential therapeutic anticancer treatment. The therapeutic potential of UPS inhibition is validated with the FDA approval of the first class proteasome inhibitor, bortezomib (VELCADE, Millenium Pharmaceuticals Inc., Cambridge, MA) which has been widely used for the treatment of multiple myeloma and the treatment of relapsed mantle cell lymphoma [12, 13]. It operates as a reversible inhibitor of the 26S proteasome [24, 57]. Although, certain cancer cell selectivity attained by reversible inhibition of 26S proteasome by bortezomib, cytotoxicity is reported as a major problem for the ubiquitination-pathway inhibition type of therapeutic approach [12, 24, 58]. Neddylation is an up-regulated pathway compared with the UPS. Therefore selective interruption in the neddylation conjugation pathway reported as a promising approach which is less associated with toxicity [11].

A significant development has been reported with the discovery of a small molecule inhibitor of Nedd8 activating enzyme (NAE) MLN4924 (Millenium by The Takeda Oncology Company) [18, 59]. MLN4924 binds to and then inhibits NAE activity, which may lead the inhibition of tumor cell proliferation and survival [13]. It has been reported that MLN4924 effectively down-regulates Nedd8 conjugation activities in vivo which results in significantly rapid loss of neddylated Cullins, specifically less than 5 minutes [60]. Knowing that the Nedd8 is overexpressed together with the CRLs showing abnormal activation in the cancer cells, Cullin neddylation inhibiton has emerged as a novel anticancer approach. The aim in blocking the Cullin neddylation is to prevent the CRL activation and thus resulting in the accumulation of substrate proteins within the cell. These proteins then trigger the cell cycle arrest, (a checkoff in the cell cycle and the cellular processes surrounding duplication and division can no longer be sustained), senescence and/or apoptosis [13, 47]. Consequently, the blockage of the Cullin neddylation pathway suppresses the tumor cell growth, specifically tumor angiogenesis in both vivo and vitro [11, 18, 21].

However; recent studies have revealed that the cancer cells begin to develop MLN4924 resistance by preferring target mutations [11, 18]. Additionally, preclinical efforts have been maintained for developing novel neddylation inhibitors by targeting Nedd8 E2s and also E3s [18]. Therefore understanding the Cullin neddylation mechanism is required for the future drug design studies for this novel anticancer approach.

3. MATERIALS AND METHODS

3.1. The Cul5^{CTD}-Rbx1 E3 Ubiquitin Ligase Structures

To achieve a mechanistic view on the neddylated Cullin dynamics, three separate systems obtained by Cul5^{CTD}-Rbx1 E3 ubiquitin ligases are studied. Two of the three states belong to the Cul5^{CTD}-Rbx1 E3 ubiquitin ligases before and after Cullin neddylation. The Cul5 based CRL crystal structure (PDB code: 3DPL, chains: C and R) represents the CRL state before neddylation whereas Nedd8-bound Cul5 based CRL crystal structure (PDB code: 3DQV, chains: A,C and R) serves as the CRL state after Cullin neddylation [20]. Figure 3.1 displays the CRL crystal structures before and after neddylation. The third system is a pseudo state (PDB code: 3DQV, chains: C and R). The Nedd8 is removed from the neddylated Cul5 based CRL crystal structure to explore CRL state after deneddylation. The structural dynamics of Cullin neddylation and its mechanism are studied via these three systems by the Molecular Dynamics (MD) simulations [61-63] in comply with the Gaussian Network Model [63-65].

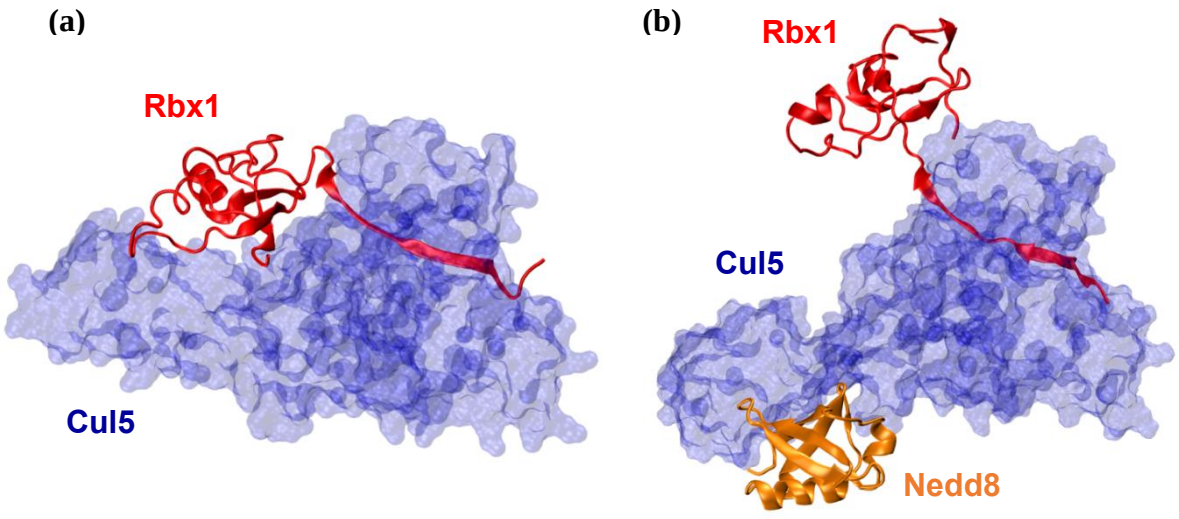

Figure 3.1. The Cul5^{CTD}-Rbx1 E3 ubiquitin ligase crystal structures. (a) unmodified-closed CRL, (b) neddylated-open CRL.

3.2. Molecular Dynamics Simulations

Molecular Dynamics simulation is a powerful computational method to study on the molecular systems and understand their time-dependent conformational changes through the simulation time. The potential energy of the systems to simulate as a function of the atomic coordinates is derived to obtain the forces acting on the system atoms throughout the simulation. Then by solving the classical Newtonian equations, which are functions of time, for each atom individually, the global dynamic motion of the system is obtained throughout the simulation time [61, 63].

Using classical mechanics instead of quantum mechanics in the MD simulations is an essential simplification to save computational power and time. The classical mechanics model the biological entities as "balls and sticks", where balls refer to the atoms and elastic sticks refer to the chemical bonds between the atoms [66]. Although the "ball and sticks" model leads less accurate results than real life results, the problem is alleviated by adopting quantum corrections as constants for classical mechanics equations.

3.2.1. Force Field

Force field includes the functions and parameters that are essential to describe the potential energy of a system of particles. The molecular mechanics force field introduced by CHARMM 27 (Chemistry at HARvard Macromolecular Mechanics) force field [62] is utilized in the MD simulations of this work.

The potential energy function of the force field is a function of the Cartesian coordinate set for N atoms and includes both bonded and non-bonded interactions. Bonded energy terms comprise of bond angles, bond lengths and torsional angles; whereas non-bonded energy terms include Lennard-Jones and Coulomb interactions [61, 66-68]. The equation of the potential function is as follows:

$$U(r_1, r_2, \dots, r_n) = \sum_{bonds} \frac{1}{2} k_l (l_i - l_{eq})^2 + \sum_{angles} \frac{1}{2} k_\theta \, (\theta_i - \theta_{eq})^2 \qquad (3.1)$$

$$+\sum_{dihedrals}\frac{1}{2}k_{\emptyset}[1+\cos(n\emptyset_i-\delta)]$$

$$+\sum_{i=1}^{N}\sum_{j=i+1}^{N}\left\{4\varepsilon_{ij}\left[\left(\frac{A_{ij}}{r_{ij}}\right)^{12}-\left(\frac{B_{ij}}{r_{ij}}\right)^{6}\right]+\left(\frac{q_iq_j}{\varepsilon r_{ij}}\right)\right\}$$

The potential energy function expressed above, in Equation 3.1 is a function of Cartesian coordinate set of N atoms, where $r_1, r_2, \dots, r_n$ represents the Cartesian coordinate vector positions. The first term of the sum for the potential energy function is the Hooke's Law (Harmonic) potential. The energy function related with the bond stretches is being calculated by the instantaneous displacements in the bond length of atom i, l_i, from the equilibrium bond length, l_{eq} in which k_l accounts for the flexible bond force constant. The second term reveals the energy function related with the bond angles, in which angle bending is also modeled as a harmonic potential. In a similar manner to the previous energy term, k_θ accounts for the angle force constant and $\theta_i - \theta_{eq}$ is the angle from equilibrium between three bonded atoms. The third energy term is associated with the torsional angles, which can also be referred as dihedrals. Dihedral force constant is represented by $k_\emptyset$. Besides, n describes the periodic nature of the function, and $\emptyset_i$ is the dihedral angle of the atom i. δ describes the phase shift. The non-bonded section of Equation 3.1 includes Van Der Waals (VDW) energy, which is calculated by 12-6 Lennard-Jones potential, and the electrostatic energy obtained by Coulomb potential. These energy terms are calculated only from the atom pairs separated by at least three bonds. Here, A_{ij} and B_{ij} are the VDW and London dispersion terms respectively. q_i and q_j represent the partial atomic charges and ε is the dielectric constant which takes the medium effect into account where the medium is expressed implicitly. However; it is usually equals to unity in a typical solvated environment due to the presence of explicit solvent [61, 66].

3.2.2. Theoretical Background of MD Simulations

The time evolution of a set of interacting atoms of the system is obtained by solving Newton's equations of motions for each system atoms and the surrounding solvent [61, 66]. Newton's equation of motion is as follows:

$$F_i = m_i a_i \tag{3.2}$$

F is the acting force on the particle i whose acceleration and mass are represented by a and m respectively. Then the acceleration of particle i is expressed in terms of the second derivative of particle position, r_i, with respect to time:

$$\frac{d^2 r_i}{dt^2} = \frac{F_i}{m_i} \tag{3.3}$$

Equation 3.1 can also be written as the gradient of the potential energy, U:

$$F_i = -\nabla U_i \tag{3.4}$$

The derivative of the potential energy is then related to the position change of the particle i as a function of time to obtain particle acceleration a:

$$\frac{d^2 r_i}{dt^2} = -\frac{1}{m_i}\frac{\partial U(r_1, r_2, \dots, r_N)}{\partial r_i} = a_i \tag{3.5}$$

Equation 3.5 requires the initial positions of the system atoms together with the initial distribution of velocities and the acceleration of the system to generate the MD simulation trajectory.

The experimental methods, X-ray or NMR (Nuclear Magnetic Resonance) spectroscopy, produce the crystal structures of the simulated systems in which the initial atom positions are well-determined. For the initial velocity distribution among the system atoms, the Maxwell-Boltzmann distribution, given in Equation 3.6, is utilized. Maxwell-Boltzmann distribution reveals the probability of atom i, p_i, whose velocity is v_x (in the x-direction) at a temperature T. The condition of no overall momentum in the system, given in Equation 3.7, corrects the Equation 3.6. Subsequently, the acceleration distribution is calculated by the gradient of the potential energy function, given in Equation 3.5.

$$p(v_{i,x}) = \sqrt{\left(\frac{m_i}{2\pi k_B T}\right)} exp\left[-\frac{1}{2}\frac{m_i v_{i,x}^2}{k_B T}\right] \tag{3.6}$$

$$p = \sum_{i=1}^{N} m_i v_i = 0 \tag{3.7}$$

The relation between the system temperature and kinetic energy is given in Equation 3.8 below, where N represents the number of atoms of the system, $\langle v_i^2 \rangle$ is the squared average velocity of the atom i and finally k_B is the Boltzmann constant [61, 69].

$$T = \frac{2}{3Nk_B} \sum_{i=1}^{N} \frac{1}{2} m_i \langle v_i^2 \rangle \tag{3.8}$$

The numerical integration of the Newton's equation of motion, Equation 3.2, aims to define the consecutive atom positions, $r_i(t + \Delta t)$ at time $t + \Delta t$ in terms of already known position $r_i(t)$ at time t. The simplicity and stability of the Verlet algorithm has made it the most commonly used integration algorithm in MD simulations. The algorithm, given in Equation 3.9, is derived from the Taylor expansions for the atom positions, $r_i(t)$.

$$r_i(t + \Delta t) = 2r_i(t) - r_i(t - \Delta t) + a_i(t)\Delta t^2 \tag{3.9}$$

In this algorithm, velocities can be calculated from the positions or propagated from explicitly as in alternative Verlet Leapfrog algorithm, which is appeared in attempt to make corrections on the original algorithm. By using an approximation for derivative, the velocity at the midpoint between the times, $t + \Delta t$ and t, is calculated as follows:

$$v_i(t) = \frac{r_i(t + \Delta t) - r_i(t - \Delta t)}{2\Delta t} \tag{3.10}$$

The outline of the described algorithm to generate MD trajectories of systems includes the following successive steps given below [66]:

- Obtaining the knowledge of initial position, $r_i(t = 0)$ of all atoms i.

- v_i assignment at the initial time of the system, that is $t = 0$, based on Boltzmann distribution at pre-defined T.
- Calculation of the position change of the atoms by $r_i(\Delta t) = r_i(t = 0) + \Delta t v_i(t = 0)$.
- Evaluation of the total potential energy function, U_i on system atoms.
- Calculation of the change in acceleration by $a_i(\Delta t) = -\frac{\nabla U_i}{m_i}$
- Verlet algorithm implementation by $r_i(t = 0)$, $r_i(\Delta t)$, and $a_i(\Delta t)$ for all atoms.
- The last 3 steps are iterated with the calculation of new atom positions for approximately 10^6 MD steps.

3.2.3. Preparation of Structures for MD Simulations

The positions of the atoms at the initial time are taken from Protein Data Bank, in a PDB text file format. In PDB text files, there may appear alternative positions to some atoms due to the inaccuracy in the crystal structure determination method. These alternative coordinates are given in order and labeled with letters. To avoid complications, the atoms having multiple positions are designated with their first alternative positions and rest is cleared from the PDB text file. Additionally, ligands and/or metals on the system residues are removed from the structure and corrected in the text file. One example is the removal of the selenium atoms from MSE (selenomethionine) residues. Another re-arrangement is the modeling the missing residues in the crystal structures. The missing residues are T64-E66 of closed-unbound-to Nedd8 state CRL's Rbx1 (PDB code: 3DPL, chain: R) and N516-K518 of open-bound-to-Nedd8 state CRL's Cul5 (PDB code: 3DQV, chain: C). The missing residues are modeled via MODELLER program [70] - Basic Modelling section by using the protein structures' homolog structures (PDB code: 3DPL, chain: Y and PDB code: 3DQV, chain: D respectively).

The re-arranged PDB text files are protonated at 310 K temperature by using MOE (Molecular Operating Environment). The protonation states of the histidine residues are determined either as HSD, HSE or HSP, depending on the side chain location.

The protonated PDB files are then utilized to generate their specific PSF files which provide all the atom-specific values. To generate the PSF files, a plug-in function in VMD (Visual Molecular Dynamics) program, named PSF Builder, is utilized. CHARMM 27 topology file [63], which includes the information of all possible conformations of atoms, bonds and angles, is adopted in the use of PSF Builder function.

3.2.4. Energy Minimization

To relieve the local stresses due to steric conflicts of non-bonded atoms, relaxing bond lengths and bond angles to their canonical values is required for refining the molecular structure. This process involves energy minimization, a non-linear optimization problem.

In energy minimization process, given the set of N independent positions $(r_1, r_2, \dots, r_N)$, the aim is to find the r_{min} where the potential energy function, U reaches its global minimum. However; the accurate positioning of the potential energy function's global minimum is impossible due to enormous number of parameters. Therefore the famous minimization methods including the gradient descent, conjugate gradient or Newton's method are being used to solve the problem.

3.2.5. Computational Details of the MD Simulations

The unneddylated and neddylated $Cul5^{CTD}$-Rbx1 E3 ubiquitin ligase structures, crystalized by the X-ray diffraction method, are taken from the Protein Databank to obtain the starting structures for the separated closed-unbound and open-bound-to-Nedd8 state CRL simulations. The Nedd8 (PDB code: 3DQV, chain: A) is then removed from the open-bound-to-Nedd8 state CRL to generate MD simulations on the pseudo-deneddylated state CRL. Explicit solvent MD simulations are performed for the three states of CRLs: closed-unbound to Nedd8 (two parallel MD simulations, 100 and 120 ns), open-bound-to-Nedd8 (3 parallel MD simulations, 100, 180 and 150 ns) and pseudo-deneddylated CRL (two parallel MD simulations, 140 and 200 ns). The details of simulated systems are given in Table 3.1.

Table 3.1. Details of the MD simulations.

System	No of Amino Acids	Simulation Time (ns)	Equilibrium Time (ns)
Closed-run1	470	100	5
Closed-run2	470	120	11
Open-run1	544	100	30
Open-run2	544	180	110
Open-run3	544	150	55
Deneddylated-run1	466	140	60
Deneddylated-run2	466	200	45

The MD simulations are performed using the NAMD 2.7 [71] program. The CHARMM 27 force field [62] is applied with 2 femtoseconds (fs) integration time step. The temperature and pressure are held constant at 310 K and 101.3 kPa, respectively by Langevin dynamics [72]. Furthermore, the covalent bonds including hydrogen atoms are kept at their equilibrium distances by SHAKE algorithm [73] usage. The initial crystal structure is then put into a TIP3P type, rectangular water box [74] with 10Å padding and neutralized with Cl- and Na+ ions. Periodic boundary conditions are also applied and Particle mesh Ewald summation [75] is used during the simulations. All systems are energetically minimized by conjugated gradient method to remove any steric crushes and crystal contacts.

3.2.6. Analysis of the MD Simulation Trajectories

The generated MD simulation trajectories are saved in every 10 picoseconds (ps) to reduce the trajectory size. Then the structural dynamics information is extracted from the reduced MD simulation trajectories. The analyses include Root Mean Square Deviation (RMSD) of atomic positions of each state from the minimized structure's, mean square fluctuations (MSF) of the residues, correlation between residue fluctuations, principal component analysis (PCA) on positional fluctuations and finally the clustering of the main conformers sampled by MD simulations.

3.2.6.1. Root Mean Square Deviation (RMSD) of Atomic Positions. RMSD of atomic positions reveals the average deviation of the atom positions in successive MD time steps. RMSD is calculated with Equation 3.11 given below.

$$RMSD_t = \sqrt{\frac{1}{N}\sum_{i=1}^{N}\left(r_{t,i} - r_{0,i}\right)^2} \tag{3.11}$$

$r_{t,i}$ represents the atomic positions of the atom i at any time t and $r_{0,i}$ shows the C_α atoms' position in the energetically minimized structure. N is the number of the C_α atoms of the simulated system.

The structures along the MD trajectories are aligned to their energetically minimized structures in every successive MD time step and RMSD values of each structure in each frame is calculated. RMSD calculation is performed by the VMD 1.9.1 program [76] plug-in function. The equilibration periods of the MD simulation trajectories are determined based on the calculated RMSD values. The other analyses are performed with the MD simulation trajectories after the specific equilibrium period in each simulated state.

3.2.3.2. Mean Square Fluctuations (MSF) of the System Residues. The physical interpretation of the mean square fluctuations (MSF) is the mobility of each system residues. It reveals the position change of each residue along the MD simulation trajectory from its mean position. MSF calculation, given in Equation 3.12, is performed only on the Cα atoms of the simulated systems where the minima and maxima fields of the MSF profile inform about its conformational structure. MSF values of the simulated system residues are calculated by the *ptraj* module of AMBER 11 [77].

$$MSF_i = \langle \Delta r_i^2 \rangle = \frac{1}{T}\sum_{t=1}^{T}\left(r_{i,t} - \bar{r}_i\right)^2 \tag{3.12}$$

where T represents the number of the frames generated by the MD simulation trajectory. $r_{i,t}$ is the position of the atom i at time t and $\bar{r}_i$ gives the average atomic position throughout the MD simulation trajectory.

3.2.3.3. Correlation between Residue Fluctuations. The cross-correlations that are the correlations between residue fluctuations expose the dynamic cross-talk between the system residues. The correlation between the residues fluctuations are calculated with Equation 3.13 given below.

$$C_{ij} = \frac{\langle \Delta r_i \Delta r_j \rangle}{\langle \Delta r_i^2 \rangle^{1/2} \langle \Delta r_j^2 \rangle^{1/2}} \tag{3.13}$$

where C_{ij} display the cross-correlation between the residues i and j. Δr_i and Δr_j represent the positional fluctuations of Cα atoms of the residues i and j, respectively.

3.2.3.4. Principal Component Analysis (PCA). Principal Component Analysis (PCA) [78] is a well-known statistical procedure using orthogonal transformation to convert a set of data of possibly correlated variables into a set of data of linearly uncorrelated variables called principal components. PCA is used to reduce the data dimension in the covariance analysis. The covariance matrix C of the positional fluctuations can be expressed as in Equation 3.14 given below.

$$\mathbf{C} = \langle (\mathbf{X} - \langle \mathbf{X} \rangle)(\mathbf{X} - \langle \mathbf{X} \rangle)^{\mathrm{T}} \rangle \tag{3.14}$$

In Equation 3.14, X represents the coordinates of N Cα atoms of the protein and has a dimension of 3N×3N, whereas $\langle X \rangle$ display the mean value of the coordinates over the equilibrated MD simulation trajectory.

The covariance matrix given in Equation 3.14 can be diagonalized as follows:

$$\mathbf{\Lambda} = \mathbf{T}^{\mathrm{T}} \mathbf{C} \mathbf{T} \tag{3.15}$$

Λ introduced in Equation 3.15 is a diagonal matrix consisting of the eigenvalues. Then the eigenvalues are sorted with respect to the data variance in which, the corresponding eigenvectors correspond to the principle components. In this work, the PCA is based on the eigenvectors that comprise of 80% of the total variance in mean positional fluctuations.

3.2.3.5. Clustering Analysis. An archetypal set of conformations can be selected among the enormous amount of conformations spanned by the MD simulations for subsequent analysis by using the clustering analysis. Clustering analysis groups the elements according to a similar measure. In MD simulations, this measure is usually the RMSD. However; clustering the MD-sampled conformations may also be based on dihedral angles and potential energies.

Table 3.2. MD simulations cluster populations.

System	**No of Clusters**	**Size of Clusters**					
		Cluster 1	Cluster 2	Cluster 3	Cluster 4	Cluster 5	Cluster 6
Closed-run1	2	955	44				
Closed-run2	2	818	381				
Closed-all	3	977	855	367			
Open-run1	3	221	376	402			
Open-run2	5	379	455	378	514	73	
Open-run3	6	143	416	135	468	93	244
Open-all	5	1270	1097	644	836	452	
Deneddylated -run1	2	602	797				
Deneddylated -run2	5	93	178	1096	507	125	

Here, Multi-scale Modeling Tools for Structural Biology (MMTSB) Tool Set's [79] *kclust* function, which uses k-means clustering algorithm, is used along with the RMSD of Cα atoms as a similarity measure. K-means clustering algorithm starts with the random election of collection of frames generated by the MD simulations and assignment of them

to their specific clusters and ends when the all frames are assigned to some specific cluster. The cluster assignment is performed according to the closeness of the cluster centroids and the frame to be clustered. When a frame is added into a cluster, the cluster centroid is re-computed. This iterative procedure continues until all the frames are equipped with a cluster. The number of the clusters depends on the selected cutoff value of RMSD as a cluster radius [80-82]. In this work, 4Å is determined as the optimum-clustering radius for closed-unbound-to Nedd8 and open-bound-to-Nedd8 state of CRLs. For the pseudo-deneddylated CRLs, clustering radius is selected as 5Å. The cluster populations are reported in Table 3.2. The details of the clustering analysis can be found in Appendix A.2.

3.3. Gaussian Network Model

Normal mode analysis (NMA) is a powerful computational method to search for the collective dynamic motions of biomolecules [83]. However; the computational difficulties of standard NMA lead the development of Elastic Network Model (ENM), a simplified normal mode analysis in which polymer network mechanics serve as a basis.

Gaussian Network Model (GNM) has emerged as the simplest ENM where the alpha carbon atoms (Cα) of each residue are modeled as nodes [64, 84]. These nodes are connected to each other by elastic springs with a uniform force constant (γ), if they are located within a cutoff distance or radius (r_{cut}) in the folded state. The fluctuations of residues are Gaussian and isotropic [64]. If the position vectors of Cα atoms of residue i and j are represented by r_i and r_j respectively, the Gaussian fluctuations can be retrieved as in the given equation below:

$$\boldsymbol{r}_{ij} = \boldsymbol{r}_i - \boldsymbol{r}_j \tag{3.16}$$

Subsequently the potential energy of a network of N residues can be calculated by:

$$U_{GNM} = \frac{\gamma}{2}\left[\sum_{i,j}^{N} \Gamma_{ij} \left(\Delta \boldsymbol{r}_i - \Delta \boldsymbol{r}_j\right)^2\right] = \frac{\gamma}{2}\left[\sum_{i,j}^{N} \Gamma_{ij} \left(\Delta \boldsymbol{r}_{ij}\right)^2\right] \tag{3.17}$$

Equation 3.17 is denoted in vector notation as follows:

$$U_{GNM} = \frac{\gamma}{2} tr[\Delta \boldsymbol{r}^T \boldsymbol{\Gamma} \Delta \boldsymbol{r}] \tag{3.18}$$

Here $\Delta \boldsymbol{r}$ represents the N-dimensional vector of the fluctuations of the individual sites. $\Delta \boldsymbol{r}^T$ is the transpose of the $\Delta \boldsymbol{r}$. Γ_{ij} stands for symmetric Kirchhoff matrix which represents the connectivity between the node i and j. It is developed by Flory *et al.* with the statistic mechanical theory of elasticity analogy [85]. The matrix is constructed by the following criteria:

$$\Gamma_{ij} = \begin{cases} -1 & i \neq j \wedge r_{ij} \leq r_{cut} \\ 0 & i \neq j \wedge r_{ij} > r_{cut} \\ -\sum_{\iota, j \neq i} \Gamma_{ij} & i = j \end{cases} \tag{3.19}$$

r_{cut} defines the cutoff radius for interacting residue range, and r_{ij} display the distance between the residues i and j. Cutoff radius is pre-determined for each mode. Reasonable cutoff radiuses embracing the all residue pairs within a first interaction shell is reported as 7.0 Å for slow modes, 6.5 Å for fast modes and 6.8 Å for average modes [86, 87]. The Figure 3.2 delineates the cutoff radius and connectivity concepts.

Then the correlation between equilibrium fluctuations of by GNM is calculated by Equation 3.20 given below.

$$\langle \Delta \boldsymbol{r}_i \cdot \Delta \boldsymbol{r}_j \rangle = \left(\frac{3 k_B T}{\gamma} \right) [\boldsymbol{\Gamma}^{-1}]_{ij} \tag{3.20}$$

where k_B is the Boltzmann constant and T is the absolute temperature in Kelvin. With the diagonalization of the connectivity matrix $\boldsymbol{\Gamma}$, Equation 3.20 becomes:

$$\langle \Delta \boldsymbol{r}_i \cdot \Delta \boldsymbol{r}_j \rangle = = \frac{3}{2} \, [\boldsymbol{U} \, \boldsymbol{\Lambda}^{-1} \boldsymbol{U}^T]_{ij} \tag{3.21}$$

$$\langle \Delta \boldsymbol{r}_i \cdot \Delta \boldsymbol{r}_j \rangle = = \frac{3}{2} \sum_k \lambda_k^{-1} (u_k)_i \, (u_k)_j \tag{3.22}$$

$$\langle \Delta \boldsymbol{r}_i \cdot \Delta \boldsymbol{r}_j \rangle_k = = \frac{3}{2} \lambda_k^{-1} (u_k)_i (u_k)_j \tag{3.23}$$

U is an orthogonal matrix, whose columns include the eigenvectors of u_k, in which the eigenvector k correspond to the residue mobility in the mode k. $\boldsymbol{\Lambda}$ is a diagonal matrix of the eigenvalues λ_k. BLZPACK [88] package is implemented as the eigensolver of the system. Due to the degrees of freedom in the simulated system, the last eigenvalue is equal to zero which leads to $N - 1$ independent eigenvalues. The eigenvalues, therefore the GNM modes, are organized in the ascending order in the $\boldsymbol{\Lambda}$ matrix. The eigenvalues reflect the frequency of motions of the corresponding mode. The slow eigenvalues correspond to the low frequency mode and thereby referred as "slow" GNM modes, whereas high eigenvalues correspond to the high frequency modes and thus referred as "fast" GNM modes. The fast GNM modes represent the localized fluctuations, whereas the slow GNM modes represent the global functional motion. The residues with high residue fluctuations are considered as computational hot spots.

The $\langle \Delta \boldsymbol{r}_i \cdot \Delta \boldsymbol{r}_j \rangle_k$ term in Equation 3.23 reveals the correlation between the residue fluctuations of the residues i and j in mode k, where λ_k is the eigenvalue and u_k is the eigenvector of the mode k. Equation 3.22 gives the cross-correlations of the residues i and j over the all modes. These correlation values vary between -1 and 1. If the two residues are auto-correlated, the correlations appear as 1 and if they are anti-correlated, the correlations appear as -1. 0 correlation value suggests that no correlation occurs between the selected two residues. Of interest, correlation values are either -1 or +1 for the case of single mode.

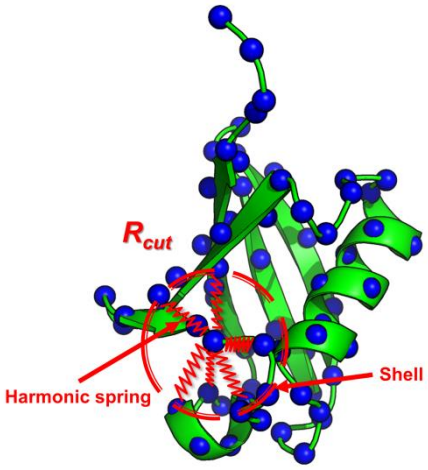

Figure 3.2. Cutoff radius representation on α-carbons of the ubiquitin protein.

Furthermore, the suppressed sites in the protein structure motion at the slowest modes behave like a bending center, hinges, which control the correlated movements of the protein. In GNM, residues showing hinge behavior also correspond to the sign change positions in the correlation. In this work, r_{cut} of 7 Å is used for the slow modes and cumulative results in the analysis of the hinge positions.

4. RESULTS AND DISCUSSION

The X-ray crystal structures of $Cul5^{CTD}$-Rbx1 complex display two different states: closed and open states (Figure 4.1). The compact structure of Cullin WHB domain with Rbx1 RING domain describes the closed state. Closed conformation is the unmodified form in which $Cul5^{CTD}$ and Rbx1 were crystalized together in the absence of Nedd8, whereas the open conformation is the modified form, the neddylated state, upon Nedd8 conjugation to $Cul5^{CTD}$. We introduced a third pseudo-state from the open conformation, where Nedd8 is removed, to possibly follow the deneddylated state of CRL machinery.

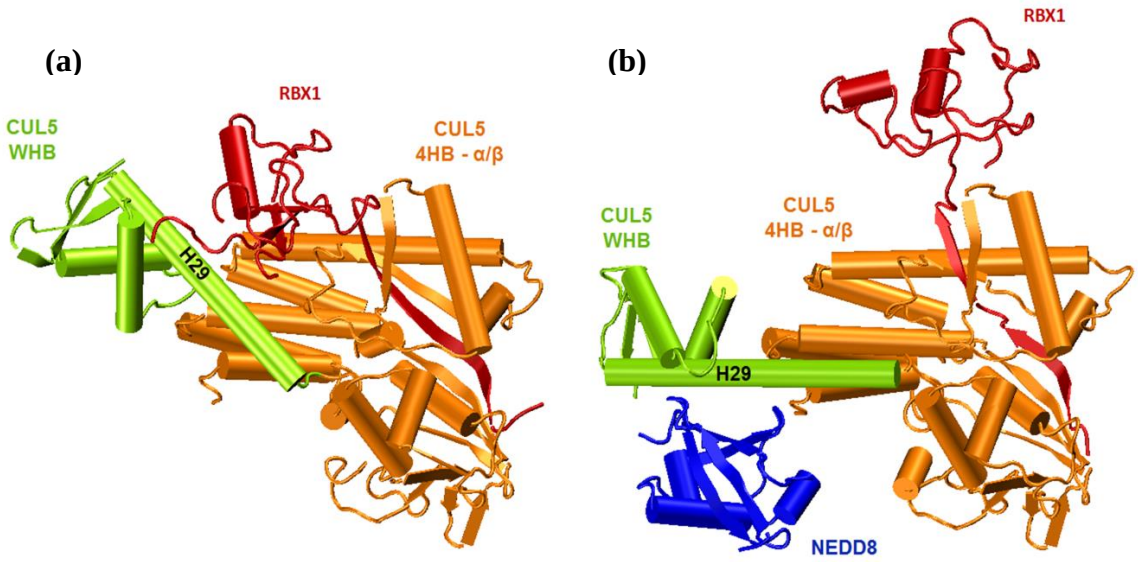

Figure 4.1. Crystal structures of the closed (a) and open (b) CRL mechanisms.

Parallel MD simulations are performed on the three different states of CRL: closed, open and pseudo deneddylated. With the ensemble of the MD sampled conformations, residue mobility profiles including the root mean square deviations (RMSD) of the atomic positions and the mean square fluctuations (MSF) of the residue positions are obtained. Figure 4.2 represents the RMSD values of the closed and open CRL systems in their performed parallel MD simulations, whereas the Figure 4.3a displays the average MSF values of the closed and open CRL system residues over the parallel MD simulation trajectories.

The RMSD profiles present the stable trajectory followed by the closed state CRLs with respect to the open-neddylated state CRLs (Figure 4.2). The average RMSD value observed in the CRL atomic positions is around 3.9 Å in the unmodified state CRL where this value increases up to 6.4 Å with the neddylation. Figure 4.3a displays the average MSF values of the closed and open state CRL structure residues over their all parallel MD simulations. The domains of each protein chains are identified just above the x-axis, where the CRL complex proteins are labelled on the top of the MSF plot. The orange stars inside the plot display the Rbx1 binding sites on Cul5, whereas the purple stars display the NEDD8-binding sites on Cul5. Furthermore, the main conformer residues of the closed (Figure 4.3b) and open (Figure 4.3c) state CRL are colored according to their normalized average MSF over their parallel runs. Further, the network of coupled residue fluctuations of the CRL complex has been explored by the cross-correlations between the residue fluctuations (Figure 4.5a and 4.5e, Figure 4.7 and Figure 4.9a and 4.9b). The dynamic information obtained from these cross-correlations will be discussed in Sections 4.2 and 4.3.

The conformations scanned through the MD simulation trajectories are clustered according to their RMSD values (Table 3.1). The most populated clusters' best member CRL complex structures are used to evaluate the relevant MD simulation trajectory and they are referred as "main conformers". The clustering details and all the cluster best members of the MD simulation trajectories are given in the Appendix A.1.

The structural alignments between the neddylated CRL main conformers, which are obtained by the individual parallel MD simulations, are superimposed to the neddylated-open CRL crystal structure from their Cul5s. Extensive Rbx1 RING domain conformations are observed in the neddylated state CRLs –compared to the unmodified form- with the rotations about the Rbx1 N-terminal β strand K20-A34, as reflected by the deviation from the initial crystal structures (Figure 4.4). In general, the Cullin neddylation increases the residue mobility of all CRL complexes, excluding the linker position, Rbx1 M50-Q67, which are significantly stabilized with NEDD8 conjugation onto Cullin (Figure 4.3a).

The Figure 4.3b and 4.3c reveal that the Cul5 WHB domain after the H29 helix and the Rbx1 RING domain are the most mobile regions of the CRL complex in both closed-

unmodified and open-neddylated state CRL with respect to the other CRL regions. In the neddylated state, Nedd8 also exhibit high mobility around the Cul5 WHB domain H29 helix, where the covalent attachment between Nedd8 and Cul5 occur. In closed CRL, the Rbx1 H1 helix is the most mobile region with respect to the other CRL regions whereas in the neddylated state CRL, Rbx1 H2 helix displays higher mobility than the Rbx1 H1 helix. The reasons of this dynamics change with the Cullin neddylation will be discussed in Section 4.1-4.3.

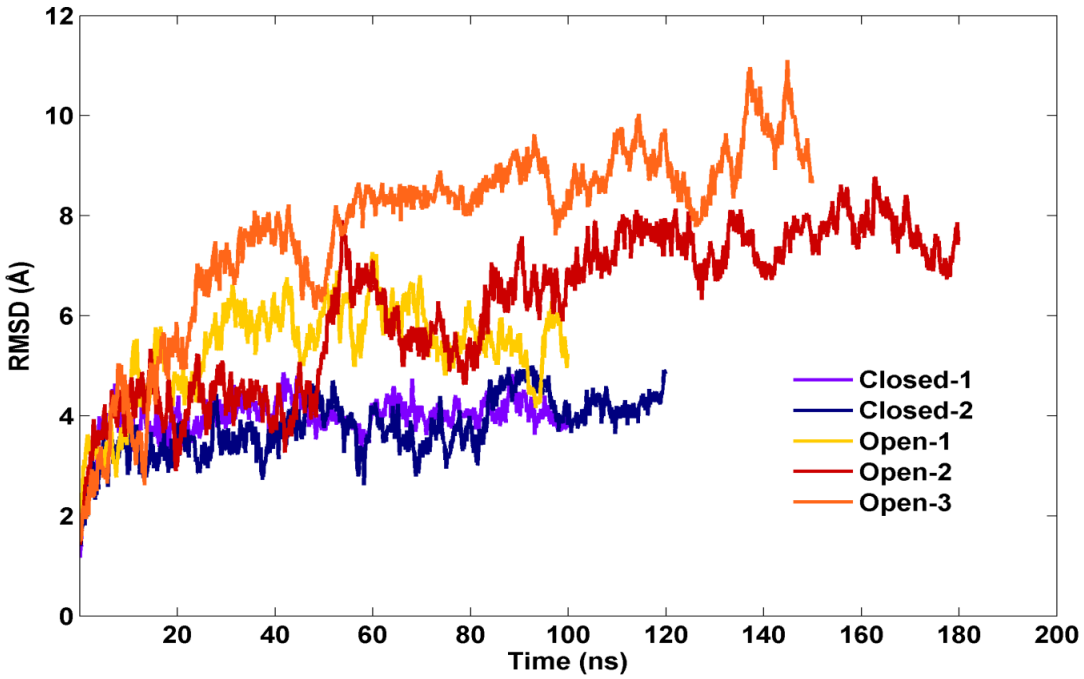

Figure 4.2. RMSD values for the simulated systems in the all parallel MD simulations.

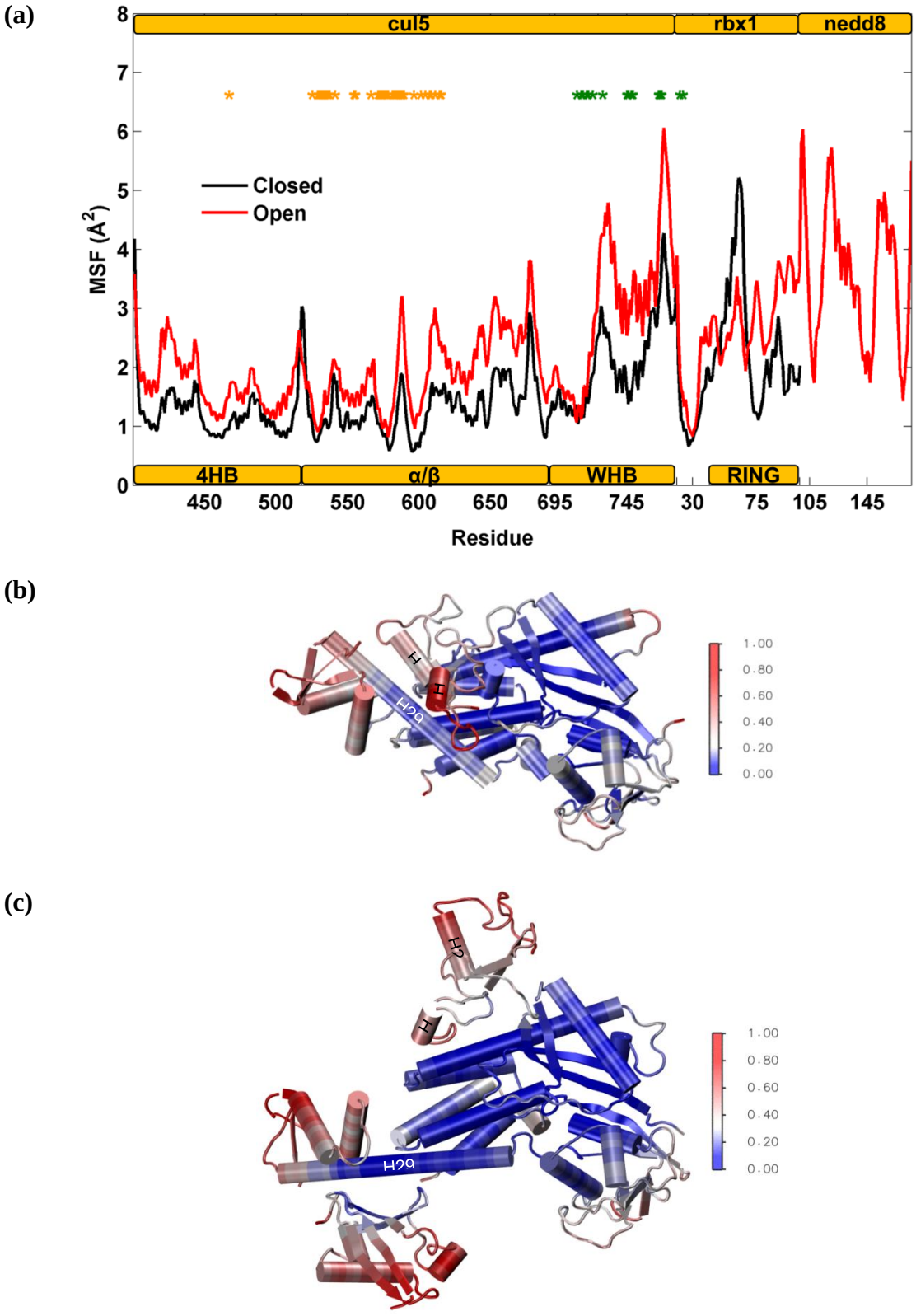

Figure 4.3. MSF values of the closed and open state CRLs over the parallel MD simulations.

4.1. Rbx1 RING domain Adopt Multiple Conformations upon Neddylation

The present MD simulations with the neddylated CRL complex structure reveal dominant multiple Rbx1 RING domain conformations about its N-terminal β strand (Figure 4.4a).

When the main conformers of the neddylated CR by three parallel MD simulations are compared, Rbx1 RING domain is observed to rotate to certain degree towards Cul5 WHB domain from the initial structure in each of these three MD runs. This rotation is measured with the Hingefind algorithm [89].

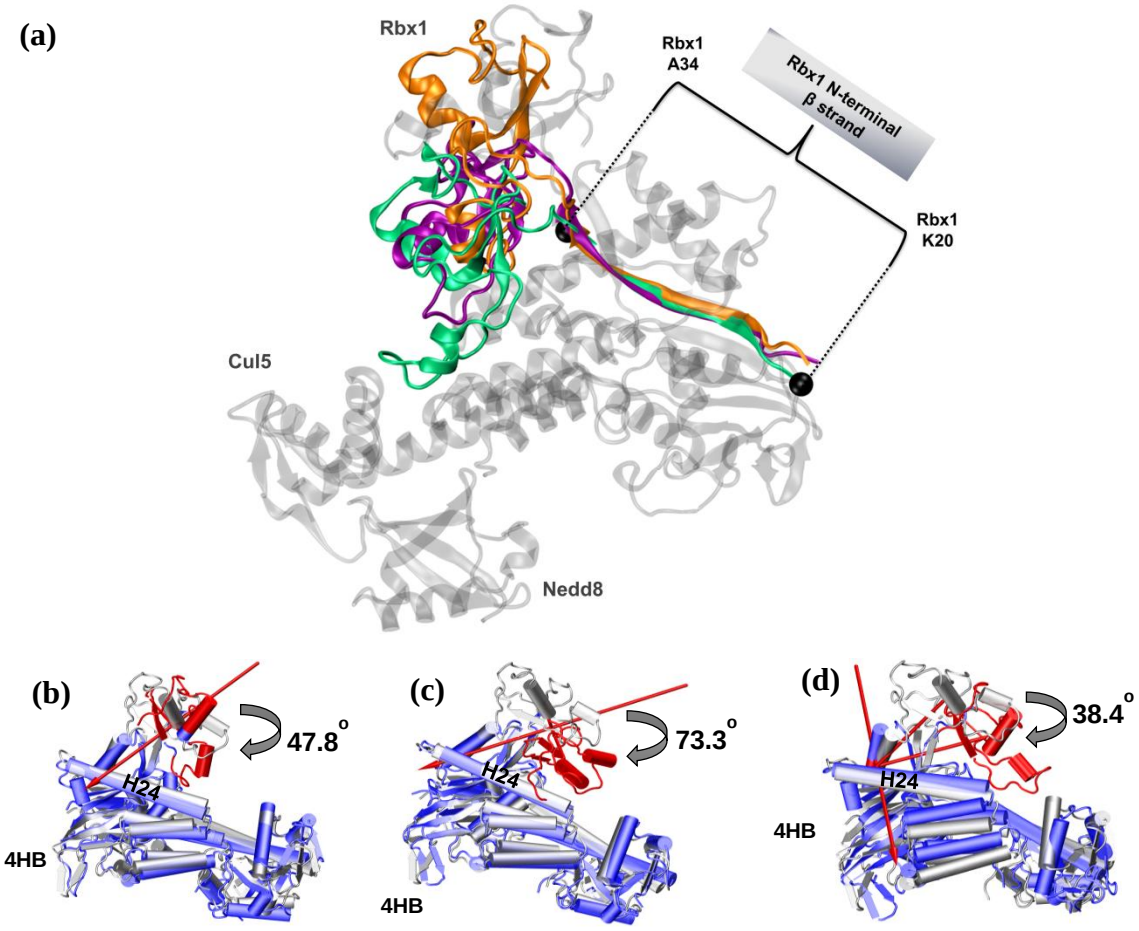

Figure 4.4. Multiple Rbx1 RING domain conformations in the neddylated state. (a) superimposition of the neddylated main conformers and crystal structure (in gray). (b), (c) and (d) individual neddylated MD simulation main conformer – Rbx1 RING rotation.

In the Hingefind algorithm, the CRL complex is partitioned into two separate domains with reasonable cutoffs. Then by the algorithm, the complex structure is fully partitioned and specific hinge residues are determined by detecting the residue positions of the domain change. According to the Hingefind algorithm, RING domain rotates 47.8^{o} about Rbx1 N41-C42 in the first, 73.3^{o} about Rbx1 V38-V39 in the second and 38.4^{o} about Rbx1 V39-D40 in the third parallel MD simulation trajectories (Figure 4.4). On the other hand, the dominant main conformer of all MD-sampled open conformations clustered together displays that Rbx1 H1 and H2 are placed almost vertical to Cul5 WHB domain with the RING domain rotation. The Rbx1 RING domain rotations will be further discussed with a metric developed from the dynamic network of the CRLs by MD simulations in Section 4.3. The rotation of Rbx1 RING domains with respect to Cul5 WHB domain possibly exposes the RING domain for an effective UBL transfer.

On the other hand, the CRL complex structure remains close to the initial structure in the unmodified CRL MD simulations except in the Rbx1 RING domain Q57-E67 region which can be also validated by the MSF values (Figure 4.3). This region includes the Rbx1 H1 first half and part of the linker before it.

Rbx1 Q57-E67 appears highly mobile, according to its MSF values (Figure 4.3), with respect to the rest of the complex structure and scans numerous conformations. The neddylation increases the residue fluctuations of all CRL structure but the Rbx1 Q57-E67 fragment, which holds the same behavior as in the unmodified state, that suggest a conserved dynamics for this fragment. Besides, the network of coupled residue fluctuations of the neddylated CRL exposes Rbx1 hinge residues at M50 and A71 that assigns the Q57-E67 fragment into a distinct dynamic domain (Figure 4.5e). The mobility of this fragment is restricted by an H-bond formation between E67 (Rbx1 RING domain)-R538 (Cul5 α/β domain) that subsequently leads to a rotation in the Rbx1 RING domain in the neddylated CRL MD simulations. The stabilizing effect of the Cullin neddylation mostly concentrates on the A61-S65 loop right before the Rbx1 H1. This loop includes S62, a residue previously proposed as critical for the conformational control upon neddylation [46].

It has recently been reported that Rbx1 RING domain conformations in CRL complexes crystalized to date (including the ones in the present work) do not have the

Rbx1 RING conformation compatible with the UBL transfer and thus do not refer to the neddylation state. An active neddylated CRL conformation requires a significant change in the Rbx1 RING domain orientation that places the Rbx1-assocatiated E2 -UBC1 - in proximity with Cullin's NEDD8 acceptor lysine [19]. The rotation in Rbx1 RING domain has thus been proposed as a general mechanism for the UBL transfer in CRL machineries. Subsequently, a CRL crystal structure (PDB code: 3RTR), with a ~60^{o} rigid body rotation in Rbx1 RING domain about a hinge centered at residues Val38 and Val39, is reported, which repositions the RING domain away from the Cul1. [90] To this end, it is suggested that observed Rbx1 conformations with RING domain rotations in the present MD simulations possibly refer towards a plausible neddylated CRL structure for an efficient ubiquitination.

Then, the next question becomes how this restriction is established. The answer is simply the arrangement of the CRL hinge residues with neddylation.

4.2. NEDD8 controls the Rbx1 Conformation via Cul5 Flexible Elements

CRLs are multi-subunit protein complexes. NEDD8 conjugation onto Cullin needs to be communicated from NEDD8 to Rbx1. MD simulations of $Cul5^{CTD}$-Rbx1-NEDD8 complex displays that there exist strong couplings between NEDD8 and Rbx1 (Figure 4.5e). These strong couplings arise from the cooperativity of Cul5 with Rbx1 and NEDD8 through the following Cul5 segments: V477-M513 in 4HB domain, I528-E541 and Y562-H574 in α/β domain, and E701-G706 in WHB domain (Figure 4.5e). These Cul5 segments lay in between the hinge residues that appear at minima in the residues' mean square fluctuations profile of this neddylated state (Figure 4.3a) and correspond to the positions where the continuity within the Cul5 dynamic domain is broken (Figure 4.5e). With this dynamic nature, these segments of Cul5 are able to dynamically associate with Rbx1 and NEDD8. We thus call these fragments as Cul5 flexible fragments.

Figure 4.5 reveals the dynamic network of the closed-unmodified and open-neddylated CRL by the average MD cross-correlations over the all parallel MD simulations. The PCA-applied cross-correlation maps obtained from the average MD simulations are shown for unmodified-closed in Figure 4.5a and neddylated-open CRL in

Figure 4.5d. The chains are separated with solid black lines in the maps and the color bar nearby them provides the scale of the correlations. The dashed lines separate the Cul5 G690-T715 region to indicate the flexible Cul5 helix H29 region where the coupled dynamics between Nedd8 and Rbx1 is coordinated. The CRL complex structures in Figure 4.5b-d are obtained by clustering all the MD-sampled closed conformers. Similarly all the open conformers spanned by the three parallel MD simulations are clustered and the main conformer for the open state CRL is obtained (Figure 4.5f-g). Figure 4.5b and Figure 4.5f are colored according to the Cul5 Leu694-Thr695 and Cul5 Glu703-Gly706 MD correlations respectively. Finally, Figure 4.5c and Figure 4.5g present the hinges obtained by the slowest GNM mode of the closed and open CRL main conformers respectively, whereas Figure 4.5d and Figure 4.5h show the CRL hinges are the GNM second slowest mode of the closed and open CRL main conformers respectively.

In Figure 4.6, the most populated clusters' main conformers of the two closed, three open and two NEDD8-removed open CRL MD simulation parallel runs are used for the GNM analysis. Figure 4.6a-g shows the hinge residues obtained by the first slowest GNM mode. Hinge residues of Rbx1 are written in green color and the encircled hinge residues are written in a box nearby the structure. Similarly, Figure 4.6h-n reveals the hinge residues obtained by the second slowest GNM mode. Furthermore, the Figure 4.6o-v emphasizes the hinge residues obtained by the second slowest GNM mode on the Cullin H29 where Nedd8 attaches on the $Cul5^{CTD}$.

Moreover, the global dynamics of $Cul5^{CTD}$-Rbx1-NEDD8 complex structure are searched by the GNM analysis of the neddylated-open CRL crystal structure together with the four neddylated-open main conformers by MD simulations: one obtained by clustering of all MD-sampled open conformations (Figure 4.5b) and three others obtained by clustering the three parallel MD-sampled open conformations individually (Figure 4.6g-o). Consequently, we observe that the Cul5 hinge residues identified by the MD simulations overlap the slowest and second slowest GNM mode hinges of the crystal structure and the four main conformers by MD. The Cul5 hinges of first and second slowest GNM mode GNM are found at F497-Q498, V502-S503, L506-N507 of 4HB domain, G534-W536, I555-P556, L571-H572, G690-L694 of α/β domain and E701-E702, E705-G706, I707-V708 of H29 helix in WHB domain (Figure 4.6g-o). The hinges of the neddylated CRL

crystal structure also covers these hinge residues. The details of the crystal structure hinges are given in the Appendix A.3.4. The set of these Cul5 hinge residues in the neddylated CRL forms the plausible flexible segments that are instrumental in providing the dynamic infrastructure for the NEDD8's allosteric communication with the Rbx1 RING domain and predisposes Rbx1 for ubiquitination. Therefore we propose that Cullin has the mediator role to transmit the signals of Cullin neddylation from NEDD8 to Rbx1.

Similarly, the hinge residues of the unmodified $Cul5^{CTD}$-Rbx1 complex are first identified by MD simulations. Then, the global dynamics of the unmodified $Cul5^{CTD}$-Rbx1 complex are analyzed by the slowest and second slowest GNM modes of the unmodified CRL crystal structure and also the main conformers obtained by clustering all the closed conformers of the two parallel MD simulations and the individual parallel MD simulations. The MD cross-correlations of unmodified $Cul5^{CTD}$-Rbx1 system display strong couplings between Cul5 and Rbx1 through the following Cul5 flexible segments: P405-A509 in 4HB domain, L531-R538, L551-G580, K613-S636 and Y650-F666 in α/β domain, L692-T696 in WHB domain (Figure 4.5a). The Cul5 hinge residues of the unmodified CRL are located at Q498-D499 of 4HB domain, I528-K529, V543-F544, D553-L554, H574-H575, L692-Q693 of α/β domain and at R714-T715, L742-K743, F746-L747 of WHB domain (Figure 4.5c-d and Figure 4.6a-f). These hinge residues are observed via GNM first and second slowest mode of the main conformer complexes. The closed CRL crystal structure also encompasses these hinges. Details related of the crystal structure hinge residues are given in Appendix A.3.4. The similarity between the closed and the open state CRL hinge residues and flexible Cul5 segments unearth the key role of the intrinsic Cul5 hinge behavior on the regulation of CRL machinery in both states.

Due to the cooperativity among the Cul5 flexible elements with Rbx1 RING (in the closed and open states) and with NEDD8 (in the open state), it is suggested that NEDD8 conjugation onto Cul5 H29 helix, re-organizes CRL mechanism to utilize the intrinsic allosteric pathways between Cul5 and Rbx1.

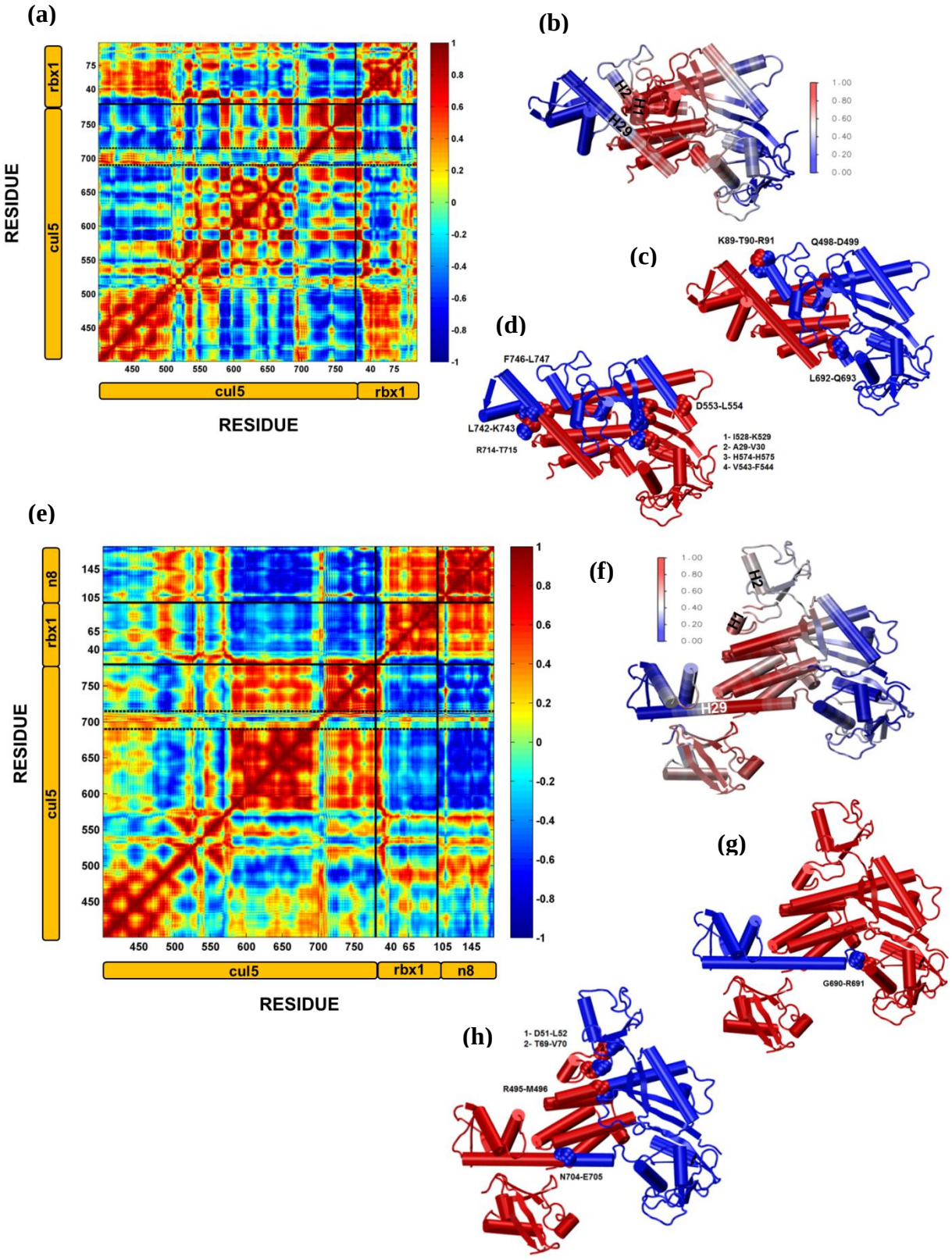

Figure 4.5. Average dynamic network of unmodified (a) and neddylated (e) state CRLs.

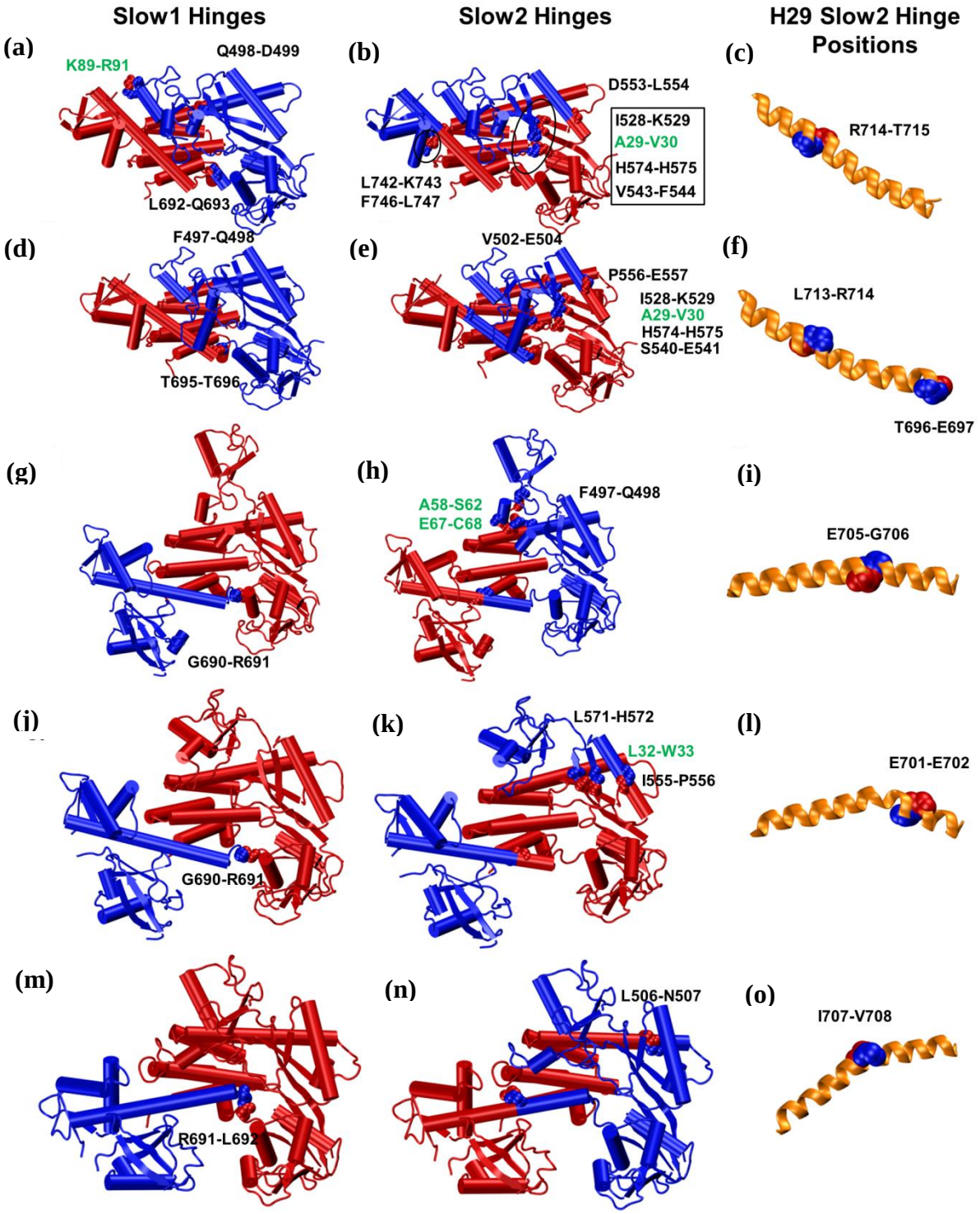

Figure 4.6. CRL hinge residues by the slowest and second slowest GNM analysis on MD simulation main conformers.

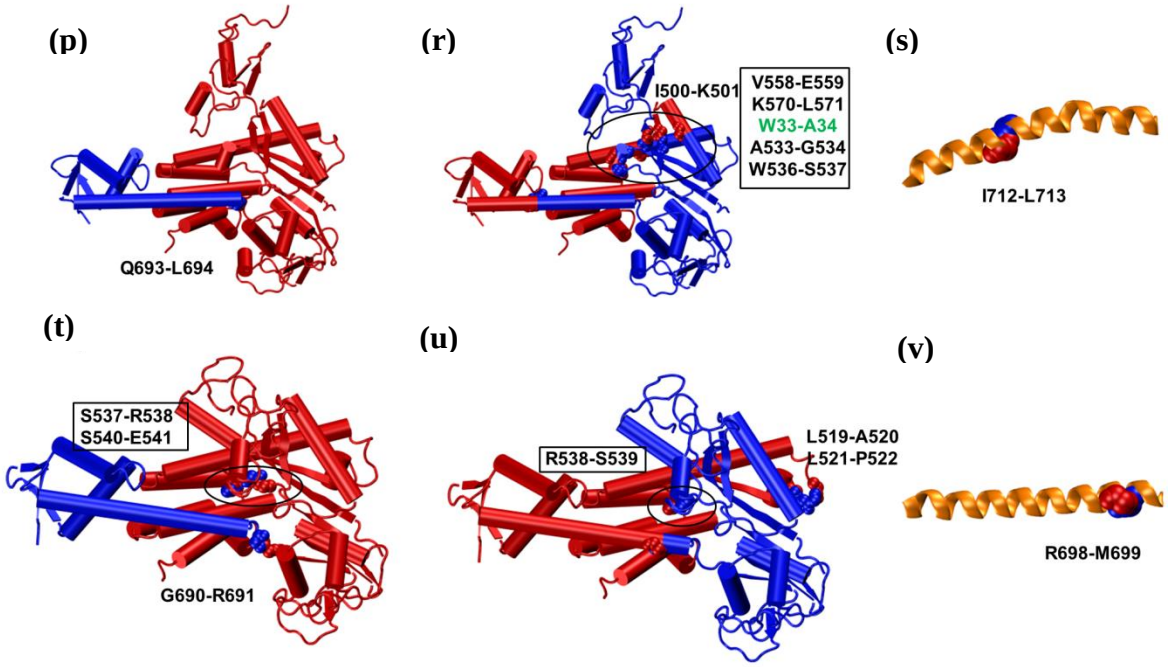

Figure 4. 6. CRL hinge residues by the slowest and second slowest GNM analysis on MD simulation main conformers cont.

4.3. A Dynamic Hinge Plane through the Flexible Cullin has the Conformational Control of Rbx1

The unmodified and neddylated CRL hinge residues are identified by residue mobility and the inter-chain cooperativity by MD simulations and observed that they overlap with the hinges coordinating the global modes of motion by the analysis of the MD main conformers. Hinge behavior on Cullin H29 helix of Cul5 WHB domain, where NEDD8 attaches on, is common in both closed and open state MD simulations (Figure 4.5a and 4.5e). In the closed state simulations' main conformers (obtained from both individual and overall parallel MD simulations), H29 helix hinge emerges on the second half of the helix at R714-T715 (Figure 4.5c).

Upon neddylation, H29 helix hinge shifts towards to the beginning of the helix, closer to the α/β domain, and positions at E705-G706, E701-E702 and I707-V708 in the first, in the second and in the third neddylated CRL parallel MD runs' main conformers respectively (Figure 4.6g-o). The neddylated-open CRL main conformer of all three MD runs has the H29 helix hinge at N704-E705 (Figure 4.6h). Besides, throughout the closed

and open state simulations, there appear kink formations in the H29 helix in both closed (kink away from Rbx1) and the open state simulations (kink toward Rbx1) (Figure 4.6a-o). The shifts in the hinge positions on H29 helix together with the kink formations prove the extended flexible nature of the Cul5 H29. Previously, a kink in Cul4A's H29 helix residues E686-Q693 has been reported to displace the Cullin WHB and Rbx1 RING domains relative to other CRLs [91]. These residues correspond to the Cul5 E705-R711 residues which validate the observed kink formations and hinge residue behaviors in the Cul5 H29 helix in the MD simulations.

In the closed state CRL simulations, the coordination of the $Cul5^{CTD}$and Rbx1 hinges of the neddylated CRL (obtained by the GNM second slowest mode of all parallel MD simulation main conformer) divides the CRL structure into two dynamic domains as if an artificial hinge plane passing through the Cul5 WHB domain H29 helix hinges (on the second half of the helix) till the Cul5 α/β domain-Rbx1 N-terminal β strand K20-A34 (Figure 4.6a-f). On the contrary, a different arrangement among the $Cul5^{CTD}$and Rbx1 hinges are attained in the neddylated-open state CRL simulations.

In the first and third parallel open state CRL simulations, the Cul5 H29 helix hinges shifts toward to the Cul5 α/β domain, positions close to the middle of the H29 helix and correlated with the hinges appearing on the Cul5 4HB domain H24. The arrangement between these hinge couples divides the neddylated CRL structure into two dynamic domains as if a hinge plane passing through the Cul5 WHB domain H29 helix hinges till the Cul5 4HB domain H24 hinges (Figure 4.6). A coupled dynamics among the Cul5 flexible elements along this imaginary hinge plane is detected (Figure 4.5f), and H-bond formations between the Rbx1 E67-either R569 (run1) or R538 (run3) of Cul5 α/β domain. In both MD runs, the H-bonds place the Rbx1 RING domain helices vertical to the Cul5 WHB domain and provide a strong allosteric communication between NEDD8 and Rbx1 RING domain as a whole (Figure 4.7c and 4.7e). Such strong cooperativity between NEDD8 and Rbx1 RING domain is also observed in the analysis of the average of all three parallel MD simulations' cross-correlations (Figure 4.5e).

On the other hand, in the second parallel run of the open state CRL simulations, the cooperativity between NEDD8 and Rbx1 is lower than the cooperativity that is observed in

other two parallel MD simulations (Figure 4.7) and the average of all MD simulations (Figure 4.5e). When the main conformer of the average MD simulations (Figure 4.5f) is analyzed by GNM, the coordination among the $Cul5^{CTD}$and Rbx1 hinges is found to be not similar to the main conformers of the other two parallel MD runs (Figure 4.6g and 4.6m). Cul5 H29 helix hinge position shifts to E701-E702. The neddylated CRL structure is divided into two dynamics domains by an imaginary hinge plane from Cul5 H29 helix through the Cul5 α/β domain obtained by the second slowest GNM mode of the neddylated main conformer as in the closed state CRL simulations. Furthermore, in addition to H-bonding of Rbx1 E67 and R538 (Cul5 α/β domain) as observed in the other parallel MD simulations, an additional H-bond formation between Rbx1 RING domain and Cul5 4HB domain (Rbx1 K105-Cul5 R481) is observed as in the closed conformation CRL. This H-bond formation restricts the Rbx1 RING domain configurational space and abrogates the rotation motion in the RING domain. The inhibition of RING domain rotation leads the RING domain adopted a conformation similar to the one in the closed state (Figure 4.8). Additionally, NEDD8-Rbx1 correlations decrease with respect to the other two parallel MD simulations. In this state of neddylated CRL, NEDD8 correlates with Rbx1 A29-C53 and S65-K89 regions (Figure 4.7d).

Consequently, one can deduce that depending on the Cul5 hinge coordination in the CRL mechanism and the hinge plane orientation, the strength of the NEDD8-Rbx1 cooperativity varies.

In Figure 4.8a, the positions of the closed and open Rbx1 RING domain of the MD-sampled conformers are determined with respect to the Cul5 and Rbx1. The x-axis shows the rotation of the RING domain about a vector tying the two edges of Rbx1 N-terminal β strand, Rbx1 K20 – Rbx1 W35. The y-axis displays the rotation of the RING domain about the axis from Cul5 N704-E705 hinges on WHB domain H29 helix to the Cul5 R495-M496 hinges on 4HB domain H24. The rotation angle with respect to the axis is determined by the angle between the relevant axis and the vector passing from Rbx1 C42 to the Rbx1 RING domain center of mass. In Figure 4.8b, the main conformers of the individual parallel MD simulations with neddylated CRL (purple as first, orange as second and lime as third parallel MD simulation main conformers) and the main conformer

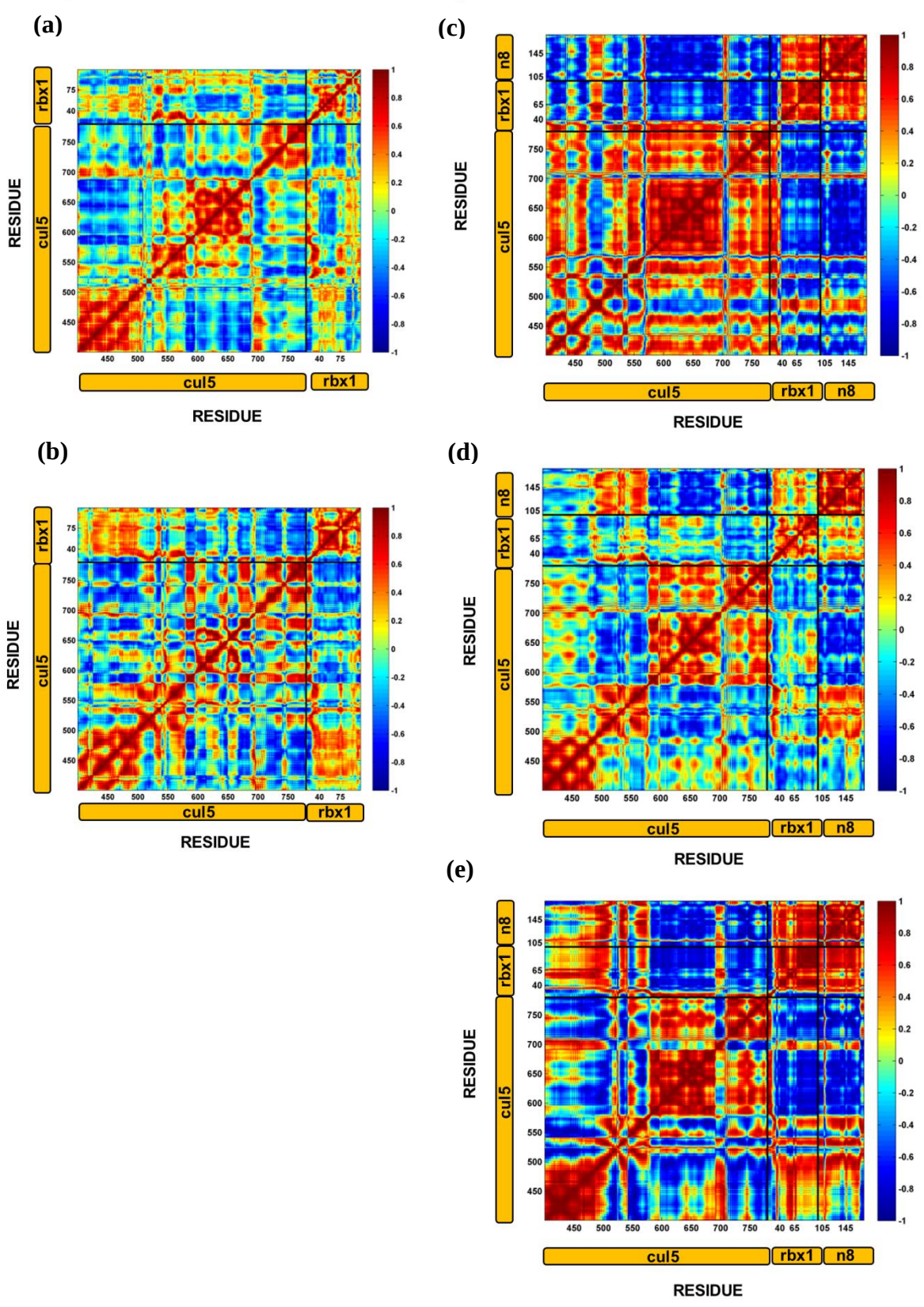

Figure 4.7. Dynamic network of individual MD parallel simulations for (a) and (b) closed-unmodified, (c), (d) and (e) open-neddylated CRL.

of the all MD-sampled neddylated CRL conformers (blue) are superimposed. The axes used in the position determination are shown with black lines.

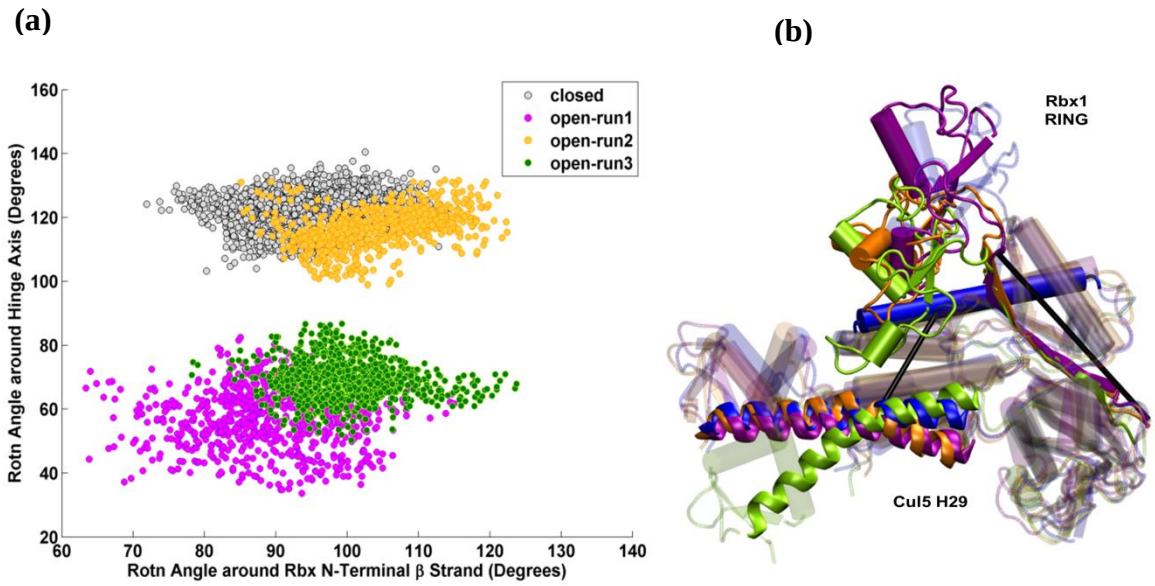

Figure 4.8. The Rbx1 RING domain positions in the neddylated state.

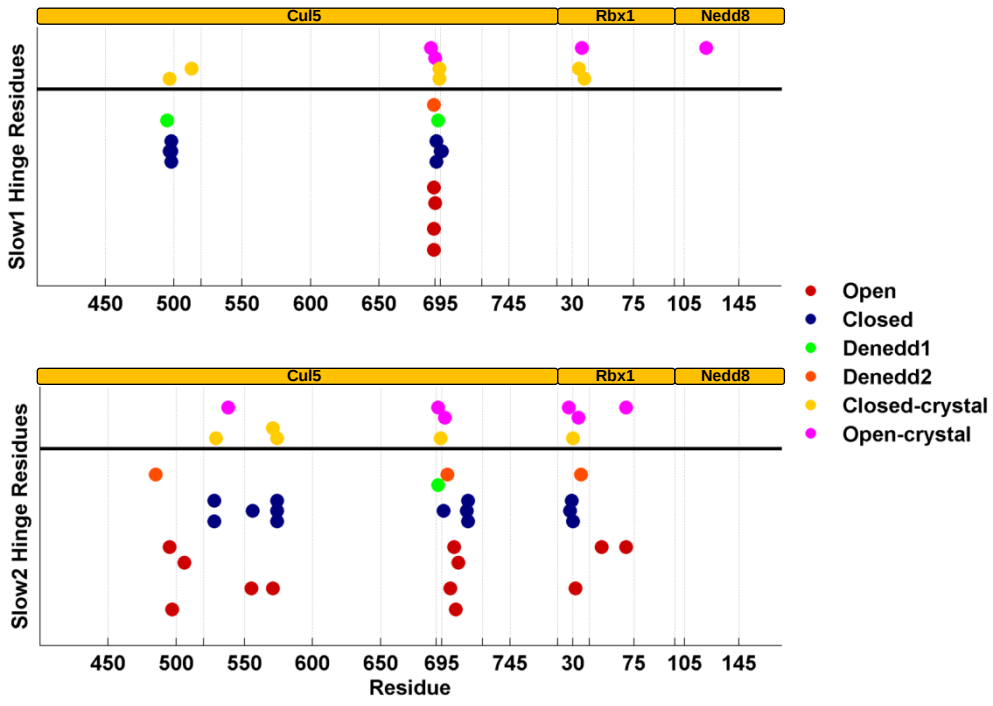

Figure 4.9. Comparison of the hinge residue positions in all states CRLs by GNM.

Figure 4.9 displays the hinge residues of the most populated cluster best members obtained from the all simulated systems, either by separate or together clustering of the parallel MD simulation conformers. Additionally, GNM analysis is performed on the crystal structures of the closed and open state CRLs as a complex and also chain by chain to gain a detailed intrinsic dynamics information. The figure proves the extended flexible nature of the Cul5 WHB domain H29 helix, which locates in between Cul5 T695-M725.

4.4. Deneddylated CRL Machinery Spans the Conformational Space between Closed and Open Conformation

From the MD simulations of open conformation-NEDD8 removed, two pseudo-intermediate states of deneddylated CRL machinery are observed. In the first parallel MD simulation, the main conformer, obtained by clustering the MD-sampled space, preserves its open conformation suggesting that the CRL-Rbx1 still sustain the NEDD8 effect on itself. Figure 4.11c represents the superimposed clusters of the first parallel MD simulation of the pseudo-deneddylated CRL, in which the open conformation persistence can be observed. On the other hand, in the second parallel MD simulation, NEDD8 effect is progressively lost. The CRL complex structure goes towards to the closed state by repositioning the Rbx1 RING domain closer to the Cul5 WHB domain. This transient stage from open to closed structure can be viewed from the superimposition of the second MD parallel simulation's clusters in Figure 4.11d. Interestingly, the Cul5 WHB domain configuration relative to the Cul5 4HB and Cul5 α/β domains is maintained as in the neddylated state (Figure 4.11c).

Residue mobility and their cooperativity are analyzed by direct analysis of MD simulation trajectories as well as the GNM for the hinge residues that coordinate the global CRL's dynamics with NEDD8 removed. The details of the pseudo-deneddylated CRL hinge residues obtained by the GNM analysis on the individual parallel MD simulations' main conformers are given in the Appendix A.3.3.

The network of coupled fluctuations in the first parallel simulation with pseudo-deneddylated CRL highly agrees that of the neddylated CRL with modest modifications on the $Cul5^{CTD}$-Rbx1 coupled dynamics. The collective dynamics of Rbx1 N-terminal β strand

with Cul5 α/β and WHB domains, which is present in the both closed and open state CRL state, is somehow lost upon deneddylation (Figure 4.11a). However, the Rbx1 RING domain E67-Cul5 α/β domain R569 H-bond holds the Rbx1 RING domain vertical with respect to the Cul5 WHB domain as in the open state.

Besides, in the first parallel MD simulation of the pseudo-deneddylated state, the Cul5 hinge coordination based on the main conformer of MD sampled conformations carries traces of the both closed and open state CRL behavior (Appendix A.3.3). The Cul5 H29 helix hinge residue appears at I712-L713 in the second half of the H29 helix of WHB domain as in the closed state. The closely positioned CRL hinge residues, Cul5 A533-G534, W536-S537, V558-E559, and K570-L571 and Rbx1 W33-A34, in the Cul5 α/β domain that are observed both in the closed and open state CRL also appear in this state of deneddylated CRL. Additionally, the hinge elucidation in the Cul5 4HB as in the neddylated CRL, where NEDD8 strongly correlates with Rbx1 RING domain, also appears in this pseudo-deneddylated state.

In the second parallel MD simulation with pseudo-deneddylated CRL, the Rbx1 RING domain approaches to the Cul5 WHB domain and CRL complex structure moves towards the closed state CRL structure. A possible transition pathway from the open-neddylated state towards the closed-unmodified state may be proposed by superimposing the all clusters' main conformers of the MD-sampled trajectory (Figure 4.11c). During this transition, Cul5 hinges are mostly concentrated around the Cul5 H29 helix beginning where all the closed and open state CRL MD sampled conformers expose a hinge residue in the Cul5 G690-T696 region (Figure 4.6t-u). The CRL hinges occurring before the H29 helix may thus be significant in the conformational control of the Cul5 WHB domain upon neddylation and deneddylation.

Additionally, the coupling between residue fluctuations reveals interplay between the Cul5 domains in the transient state of deneddylated CRL obtained in the second parallel MD simulation. The two edges of $Cul5^{CTD}$, Cul5 α/β domain and Cul5 WHB domain, are dynamically coupled in the both closed and open state CRL MD simulations (Figure 4.7a and 4.7e). These couplings between these two Cul5 domains are consolidated with neddylation, especially in the case of the strong NEDD8-Rbx1 collectivity. Yet, with

the deneddylation, the Cul5 WHB domain abandons this coupling to couple with the α/β domain and correlates with Cul5 4HB domain (Figure 4.11b).

The complex behavior of the deneddylated CRL states in between the closed and open state CRL can also be observed with the Cul5 WHB conformational change upon deneddylation. Upon neddylation and thus the conformational change in Cul5 WHB domain, E740-L747 loop of the Cul5 WHB forms strong couplings with NEDD8 L108-T109 residues (Figure 4.5e). As NEDD8 is removed, the Cul5 WHB domains of the deneddylated CRL main conformers start going back to its initial conformational space as in the unmodified-closed state position (Figure 4.11f). High RMSD (Figure 4.10a) and MSF (Figure 4.10b) values are obtained in the second MD parallel simulation's deneddylated CRL conformers due to the significant conformational changes towards to the closed CRL structure, representing the transient stage between the closed and open CRL conformation. Additionally, the main conformers of the individual parallel MD simulations (Figure 4.10c as first and 4.10d as second), that are colored according to the normalized MSF values; agree in the CRL regions showing high mobility with respect to the overall complex structure. These regions are the Rbx1 RING domain and the Cul5 WHB domain after the second half of the Cul5 H29 helix, where the conformational changes occur upon Cullin neddylation. Observing high RMSD and MSF values in the second parallel MD simulation main conformer (Figure 4.10d) supports the transient stage behavior of the deneddylated CRL.

Finally, the Rbx1 RING domain positions in the deneddylated state are analyzed with respect to the equal metric used in Figure 4.8 (Figure 4.11e). In Figure 4.11e, the Rbx1 RING domain of the first parallel MD simulation conformers (orange spots), which preserves the Nedd8 effect, positions close to the neddylated-open CRL state Rbx1 RING domain position where strong coupling between Nedd8 and Rbx1 (red spots) is observed. On the other hand, the second parallel MD simulation conformers' Rbx1 RING domains scan a large conformational space between the closed and open state supporting the premise of the possible transient pathway between the two end's CRL conformations.

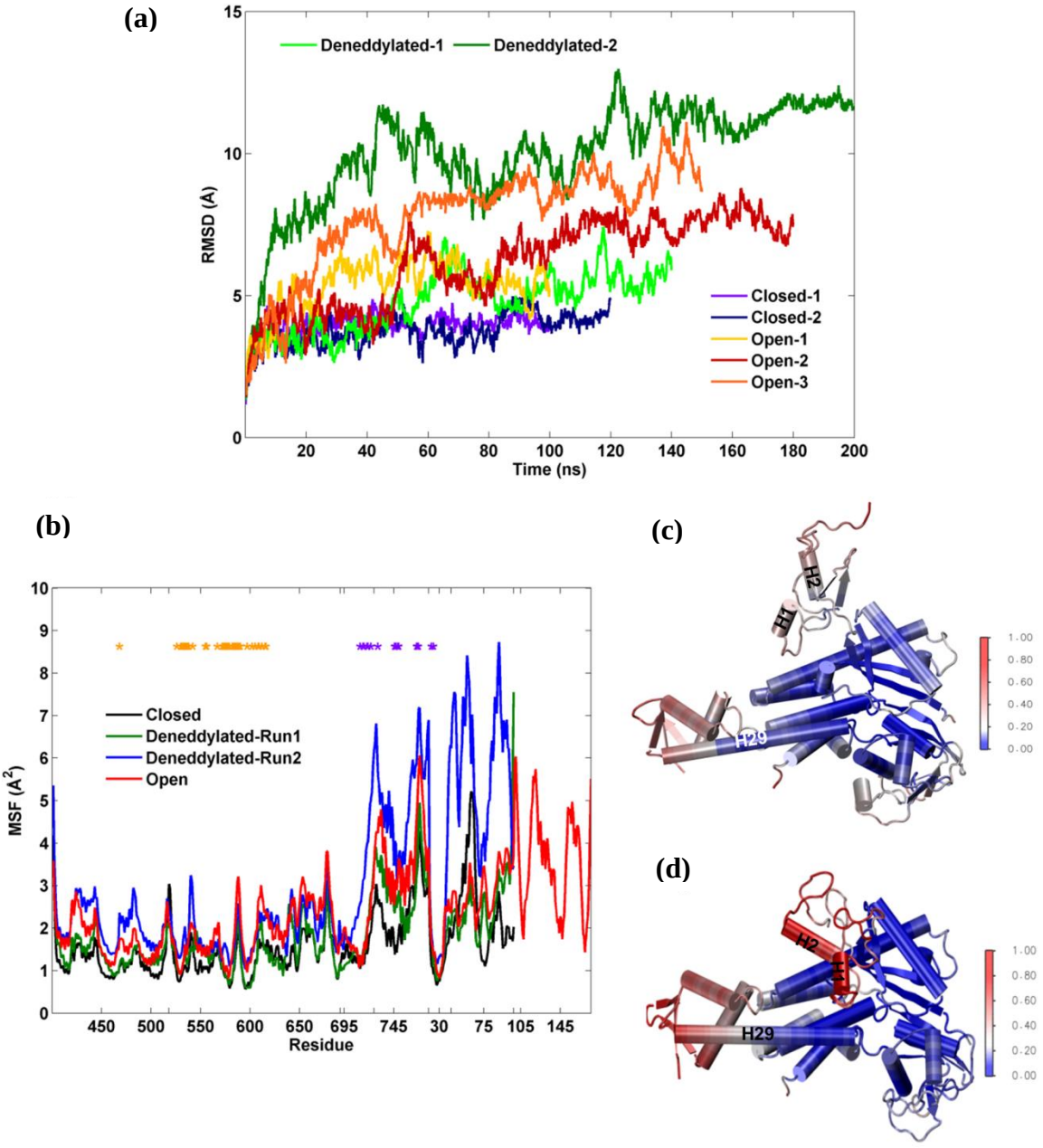

Figure 4.10. The RMSD and MSF profiles of pseudo-deneddylated state CRLs.

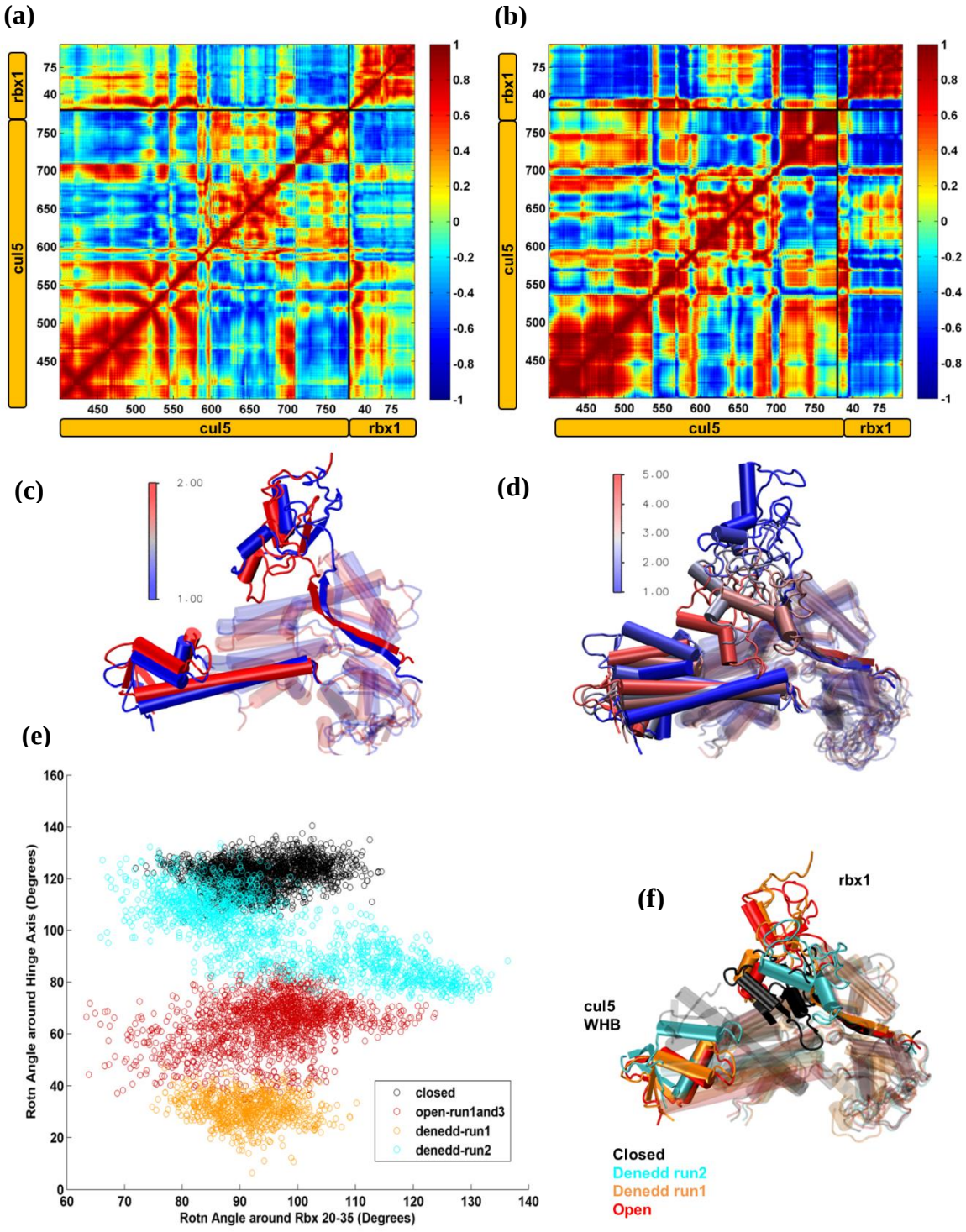

Figure 4.11. Deneddylated CRL dynamics.

5. CONCLUSIONS AND RECOMMENDATIONS

5.1. Conclusions

Cullin neddylation stimulates the Cullin-RING E3 ligase activity by leading significant conformational changes in the Cullin CTDs. CRLs hold a substrate protein on one arm and ubiquitin or ubiquitin-like protein, Nedd8, on the other arm. With neddylation, conformation change in Cullin WHB domain together with the RING domain of the E3 ligase potentially closes the gap between the two ends of the CRL mechanism and thereby facilitates the ubiquitination. Understanding the Cullin neddylation effect on the structural dynamics of Cullin-RING E3 ligases and providing a detailed mechanistic view on the process is essential in terms of generating useful information for the novel anticancer therapeutic approach, which is inhibiting the Cullin neddylation pathway. In this scope; the structural dynamics of $Cul5^{CTD}$-Rbx1 RING E3 ligases before and after Cullin neddylation and also after deneddylation are investigated by MD simulations and Gaussian Network Model.

The results reveal that the rigorous nature of unmodified CRL structure is thwarted with the Cullin neddylation. With neddylation, Rbx1 moves away from the Cul5 WHB domain and spans a large conformational space. The conformational control of the Rbx1 is provided by Nedd8 due to the discovered allosteric communication between the Rbx1 and Nedd8. Nedd8 predisposes Rbx1 for effective ubiquitin transfer by leading significant rotations in the Rbx1 RING domain [90]. With RING domain rotations, Rbx1 adopts proposed neddylated state conformations in the MD simulations by closing the gap between the E3 RING domain and the Cullin acceptor lysine.

To date, the effect of Cullin neddylation on the CRLs are studied from the perspective of Nedd8 and Rbx1 flexibility. In this thesis, the main focus is Cul5, the scaffold member of the CRL complex, which lies between the Nedd8 and Rbx1. Cul5 may be a significant mediator protein in transmitting the signals of Cullin neddylation to the Rbx1 and interceding the allosteric conformational control of Rbx1 by Nedd8. This mechanism is anticipated in the allosteric communications in the multi-subunit complex

structures [16]. This idea is supported with the MD simulation cross-correlations that display the cooperativity of Cul5 with Rbx1 and Nedd8 through the Cul5 flexible segments. These segments remain between the Cul5 hinges obtained by GNM analysis on the MD simulations main conformers. Of interest, GNM slowest and second slowest mode of MD simulation main conformers cover the hinge residues observed in the MD cross-correlations, which suggests that the first two GNM mode may represent the global mode of the CRL structure in MD simulations.

Moreover, a dynamic hinge plane of Cul5 hinges at R495-M496, N704-E705 and Rbx1 hinges at D51-L52, T69-V70 is proposed to coordinate the allosteric communication between Nedd8 and Rbx1 on the CRL structure together with an H-bond between Cul5 R538, R569 and Rbx1 E67 which narrows the Rbx1 conformational space. The dynamic hinge plane can be a conceivable mechanism clarifying the allosteric conformational control of Rbx1.

On the other hand, MD simulations reveal a combined dynamics of the closed and open state CRL on the deneddylated systems. Conjugation of Nedd8 to Cul5 H29 helix and interaction between Nedd8 and Cul5 H29 helix hinge region may be responsible from the dynamic hinge plane formation and orientation. Upon deneddylation, the CRL hinges may not become coordinated in a distinctive way as observed in the closed and open state CRLs. Thereby a complex state between the closed and open states appears in the deneddylated state CRLs. One parallel MD simulation prefers to sustain the Nedd8 effect and the other get rids of the Nedd8 effect and goes back to the closed CRL conformation. The transient conformations obtained in the parallel MD simulations of deneddylated CRL that prefers to go back to the closed state, may reveal an elucidative pathway from the open-neddylated state to the closed-unmodified state.

5.2. Recommendations

The effectiveness measure of the obtained neddylated-open CRL main conformers' conformations can be searched by the docking studies of E2 enzyme-carrying Nedd8 on the E3 RING ligase. With the rotated Rbx1 RING domains observed in the neddylated CRL state, the distance between the Nedd8 on the E2-enzyme and the Cullin acceptor

lysine on its C-terminal domain is expected to decrease. The closure of the gap between these proteins facilitates the Cullin neddylation. Therefore to understand the extent of the Nedd8's control on the CRL mechanism by Cullin neddylation, docking of Nedd8-carrying E2 enzyme onto the E3 RING ligase is strongly recommended.

Furthermore, the significant Cul5 and Rbx1 hinge residues for the proposed dynamic hinge plane can be mutated to further elaborate the suggested plausible mechanism's effect on the CRL complex structure dynamics.

In this thesis, the effect of Cullin neddylation is studied on the C-terminal domain of the Cullin-RING E3 ligases. To attain the complete picture, modeling the complete Cul5 and then performing MD simulations is highly recommended. Although higher computational power and time is required to simulate the modelled Cul5-RING E3 ligase system, any possible structural dynamics information extracted would be valuable for the allosteric drug design studies on Cullin neddylation inhibition.

APPENDIX

A.1. MSF Profiles of the Individual Parallel MD Simulations

The orange and green stars given in the below MSF profiles represent Rbx1 and Nedd8 binding sites on Cul5.

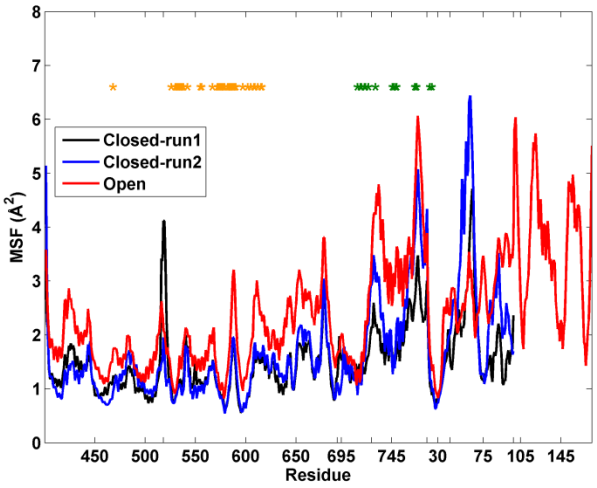

Figure A.1. MSF profile of the individual parallel MD simulations of closed state CRLs compared with the average open state CRL MSFs.

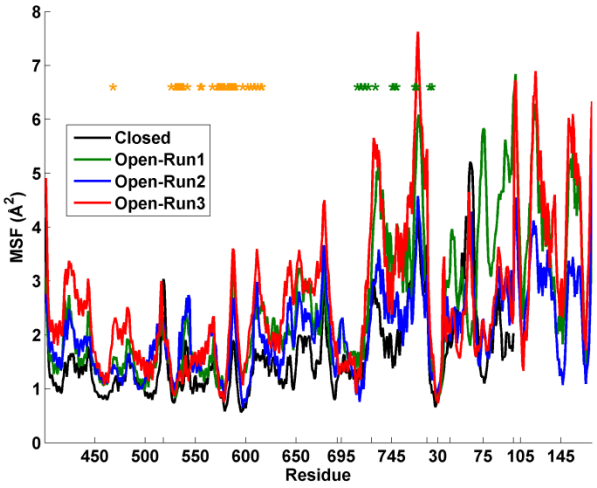

Figure A.2. MSF profile of the individual parallel MD simulations of open state CRLs compared with the average closed state CRL MSFs.

A.2. Cluster Analysis

The cluster sizes and the RMSD distribution for each cluster can be found in the figures below.

A.2.1. Closed-Unmodified CRLs

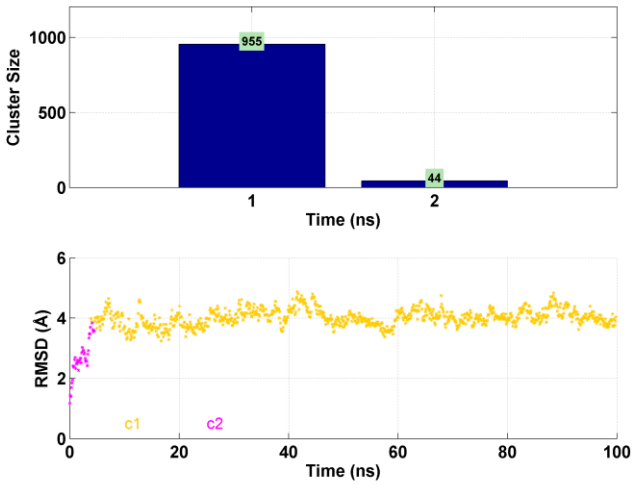

Figure A.3. Individual clusters distribution on RMSD profile for first parallel MD simulation with closed state CRL.

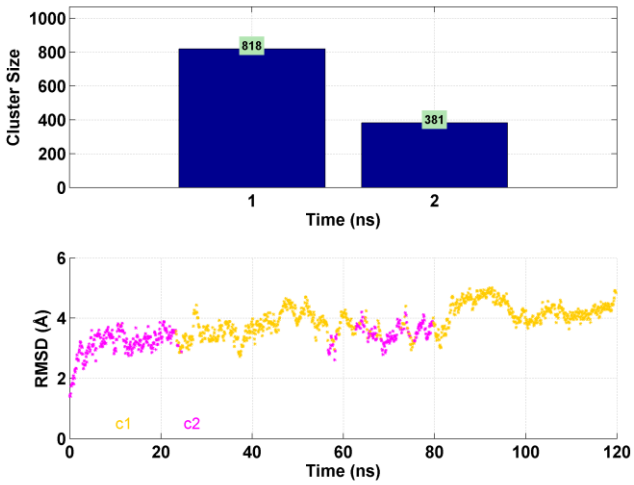

Figure A.4. Individual clusters distribution on RMSD profile for second parallel MD simulation with closed state CRL.

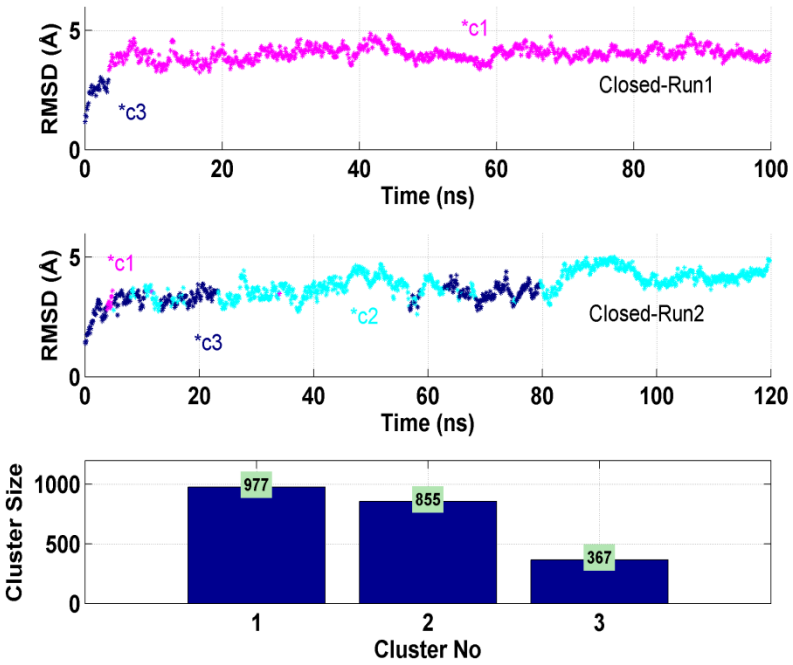

Figure A.5. Clustering over the all parallel MD simulation closed state CRL conformers.

A.2.2. Open-Neddylated CRLs

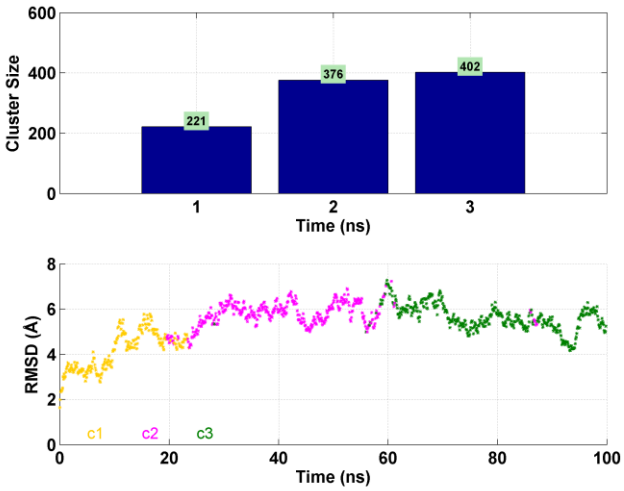

Figure A.6. Individual clusters distribution on RMSD profile for first parallel MD simulation with open state CRL.

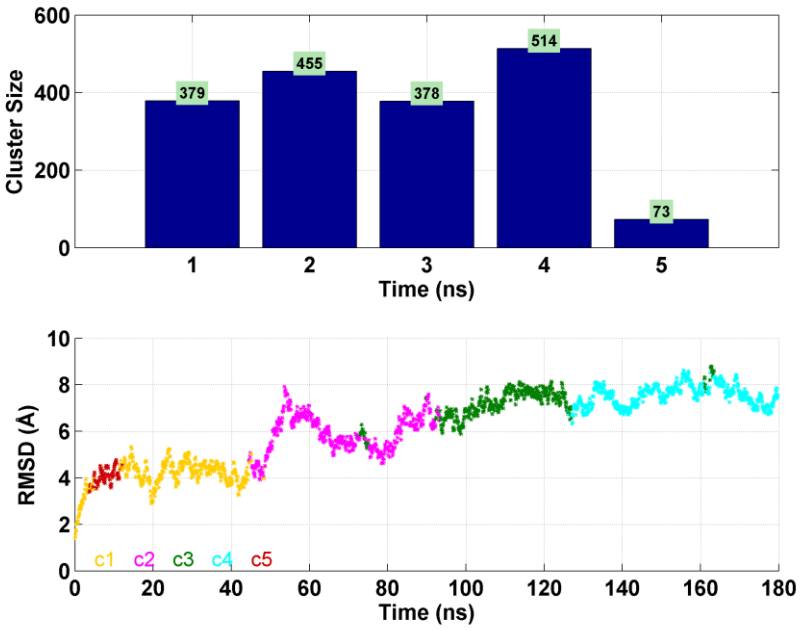

Figure A.7. Individual clusters distribution on RMSD profile for second parallel MD simulation with open state CRL.

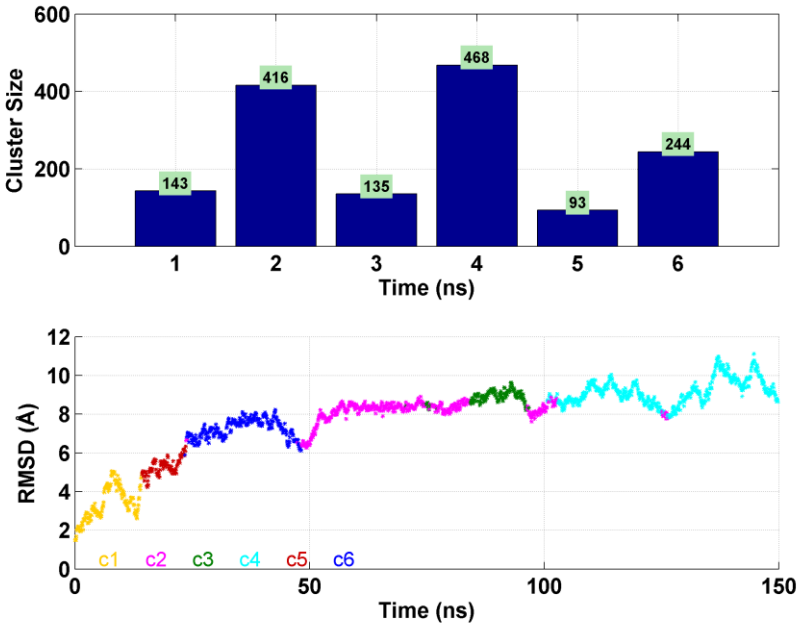

Figure A.8. Individual clusters distribution on RMSD profile for third parallel MD simulation with open state CRL.

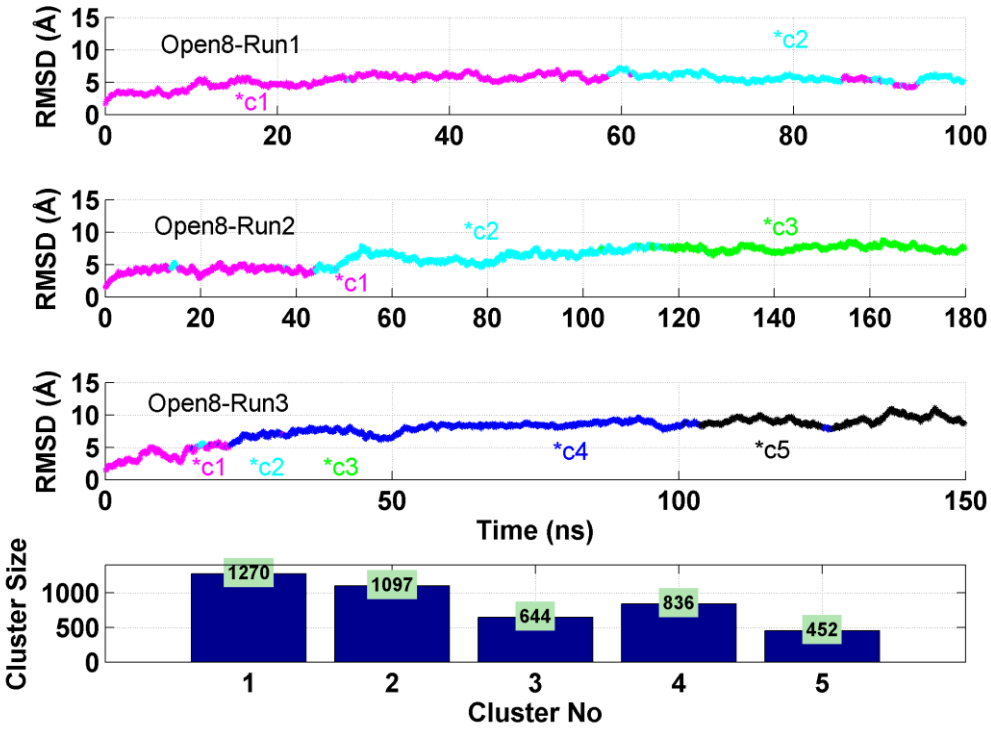

Figure A.9. Clustering over the all parallel MD simulation open state CRL conformers.

A.2.3. Pseudo-Deneddylated CRLs

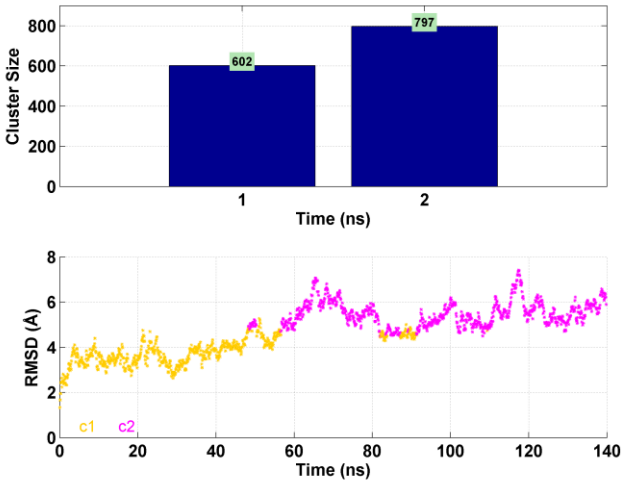

Figure A.10. Individual clusters distribution on RMSD profile for first parallel MD simulation with pseudo-deneddylated state CRL.

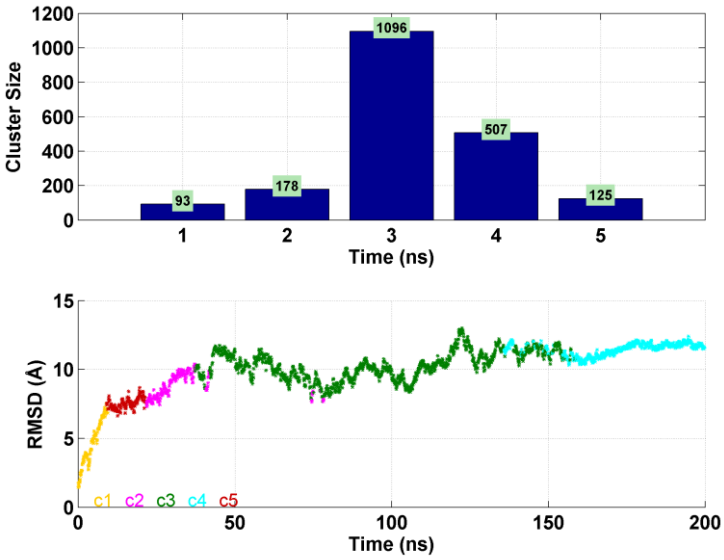

Figure A.11. Individual clusters distribution on RMSD profile for second parallel MD simulation with pseudo-deneddylated state CRL.

A.3. GNM Analysis

A.3.1. Closed-Unmodified CRLs

Table A.1. The slowest and second slowest GNM mode hinges of unmodified-closed CRL main conformers.

Closed State CRL							
1st Slowest GNM Mode Hinges				2nd Slowest GNM Mode Hinges			
	Run1	**Run2**	**Avg**		**Run1**	**Run2**	**Avg**
Cul5	Q498	F497	Q498	**Cul5**	I528	V502	I528
	D499	Q498	D499		K529	S503	K529
	L692	T695	L692		V543	E504	V543
	Q693	T696	Q693		F544	I528	F544
					D553	K529	D553
					L554	S540	L554
					H574	E541	H574
					H575	P556	H575

					R714	E557	R714
					T715	H574	T715
					L742	H575	L742
					K743	T696	K743
					F746	E697	F746
					L747	L713	L747
						R714	
Rbx1	K89		K89	**Rbx1**	A29	A29	A29
	T90		T90		V30	V30	V30
	R91		R91				

A.3.2. Open-Neddylated CRLs

Table A.2. The slowest and second slowest GNM mode hinges of neddylated-open CRL main conformers.

Open State CRL									
1st Slowest GNM Mode Hinges					2nd Slowest GNM Mode Hinges				
	Run1	**Run2**	**Run3**	**Avg**		**Run1**	**Run2**	**Run3**	**Avg**
Cul5	G690	G690	R691	G690	**Cul5**	F497	I555	L506	R495
	R691	R691	L692	R691		Q498	P556	N507	M496
						E705	L571	I707	N704
						G706	H572	V708	E705
							E701		
							E702		
					Rbx1	A58	L32		D51
						N59	W33		L52
						Q60			T69
						A61			V70
						S62			
						E67-C68			

A.3.3. Pseudo-Deneddylated CRLs

Table A.3. The slowest and second slowest GNM mode hinges of pseudo-deneddylated CRL main conformers.

Pseudo-Deneddylated State CRL					
1st Slowest GNM Mode Hinges			2nd Slowest GNM Mode Hinges		
	Run1	**Run2**		**Run1**	**Run2**
Cul5	Q693	S537	**Cul5**	I500	L519
	N694	R538		K501	A520
		S540		G533	L521
		E541		A534	P522
		G690		W536	R538
		R691		S537	S539
				V558	R698
				E559	M699
				L570	
				K571	
				I712	
				L713	
			Rbx1	W33	
				A34	

A.3.4. Crystal Structures

A.3.4.1. Closed-Unmodified CRLs

Table A.4. The slowest and second slowest GNM mode hinges of unmodified-closed CRL crystal structure.

Closed State			
1st Slowest GNM Mode Hinges		2nd Slowest GNM Mode Hinges	
Analysis on CRL	Analysis on Separate	Analysis on CRL	Analysis on Separate

complex		Chains		complex		Chains	
Cul5	Rbx1	Cul5	Rbx1	Cul5	Rbx1	Cul5	Rbx1
L462	A34	I463		K542	N28	K542	V24
I463	W35	L464		V543	A29	V543	K25
L464		D465		E552	E55	T549	N41
D465		Q498		D553	C56	E550	C42
D499		D499		H575	E67	H574	C75
I500		G534		L576	C68	H575	N76
I531		A535		M577		L576	
N532		W536		S578		M577	
S540		S537		N579		S578	
E541		T696		L692		N579	
T696		E697		Q693		L692	
E697				Q709		Q693	
				L710		V708	
						Q709	
						K743	
						N744	
						M745	
						F746	

A.3.4.2. Open-Neddylated CRLs

Table A.5. The slowest and second slowest GNM mode hinges of neddylated-open CRL crystal structure.

Open State									
1st Slowest GNM Mode Hinges					2nd Slowest GNM Mode Hinges				
Analysis on CRL complex		Analysis on Separate Chains			Analysis on CRL complex		Analysis on Separate Chains		
Cul5	Rbx1	Cul5	Rbx1	Nedd8	Cul5	Rbx1	Cul5	Rbx1	Nedd8
N410		L415	D36	K106	E559	W33	S540	K26	L102
Y411		L416	I37	T107	E560	A34	E541	W27	I103

E436		K423		K111	F561		T549	N41	I115
V437		K424		E112	Y562		E550	C42	D116
Y453		H454		I126	K570		H574	N47	Q141
H454		K455		K127	L571		H575	H48	R142
T696		V477		L143	E703		L576	M50	Q149
E697		E478		I144	N704		M577	D51	M150
		P486		L167			S578		M162
		A487		H168			N579		G163
		E697					R691		L171
		R698					L692		A172
							Q693		
							L694		
							T696		
							E697		
							E703		
							N704		
							E705		
							G706		

A.4. Sequence Alignment Results for Cul4A and Cul5

The sequence alignment is performed between Cul4 (PDB code: 2HYE, chain: C) and Cul5 (PDB code: 3DQV, chain: C) to check the correspondence of the Cul4 residues forming kinks on H29 helix in Cul5. The results are given below:

```
CLUSTAL 2.1 multiple sequence alignment


2HYE_C|PDBID|CHAIN|SEQUENCE
MADEAPRKGSFSALVGRTNGLTKPAALAAAPAKPGGAGGSKKLVIKNFRD 50
3DQV_C|PDBID|CHAIN|SEQUENCE       ----------------------------------------------
----


2HYE_C|PDBID|CHAIN|SEQUENCE
RPRLPDNYTQDTWRKLHEAVRAVQSSTSIRYNLEELYQAVENLCSHKVSP 100
3DQV_C|PDBID|CHAIN|SEQUENCE       ----------------------------------------------
----
```

```
2HYE_C|PDBID|CHAIN|SEQUENCE
MLYKQLRQACEDHVQAQILPFREDSLDSVLFLKKINTCWQDHCRQMIMIR 150
3DQV_C|PDBID|CHAIN|SEQUENCE       ----------------------------------------------
----


2HYE_C|PDBID|CHAIN|SEQUENCE
SIFLFLDRTYVLQNSTLPSIWDMGLELFRTHIISDKMVQSKTIDGILLLI 200
3DQV_C|PDBID|CHAIN|SEQUENCE       ----------------------------------------------
----


2HYE_C|PDBID|CHAIN|SEQUENCE
ERERSGEAVDRSLLRSLLGMLSDLQVYKDSFELKFLEETNCLYAAEGQRL 250
3DQV_C|PDBID|CHAIN|SEQUENCE       ----------------------------------------------
----


2HYE_C|PDBID|CHAIN|SEQUENCE
MQEREVPEYLNHVSKRLEEEGDRVITYLDHSTQKPLIACVEKQLLGEHLT 300
3DQV_C|PDBID|CHAIN|SEQUENCE       ----------------------------------------------
----


2HYE_C|PDBID|CHAIN|SEQUENCE
AILQKGLDHLLDENRVPDLAQMYQLFSRVRGGQQALLQHWSEYIKTFGTA 350
3DQV_C|PDBID|CHAIN|SEQUENCE       ----------------------------------------------
----


2HYE_C|PDBID|CHAIN|SEQUENCE
IVINPEKDKDMVQDLLDFKDKVDHVIEVCFQKNERFVNLMKESFETFINK 400
3DQV_C|PDBID|CHAIN|SEQUENCE       ----------------------------------------------
---G 1


2HYE_C|PDBID|CHAIN|SEQUENCE                                RPNKPAELIAKHVDSKLRAG--
NKEATDEELERTLDKIMILFRFIHGKDV 448
3DQV_C|PDBID|CHAIN|SEQUENCE
SESKCPEELANYCDMLLRKTPLSKKLTSEEIEAKLKEVLKKLKYVQNKDV 51
                                  .*  .*  :*::  *    **       .*:  *.**:*  .*.:::
::::::***

2HYE_C|PDBID|CHAIN|SEQUENCE               FEAFYKKDLAKRLLVGKSASVDAEKSMLSKLKHECG-
AAFTSKLEGMFKD 497
3DQV_C|PDBID|CHAIN|SEQUENCE
FMRYHKAHLTRRLILDISADSEIEENMVEWLREVGMPADYVNKLARMFQD 101
                                *   ::* .*::**::. **. : *:.*:. *:.     * :..**
**:*

2HYE_C|PDBID|CHAIN|SEQUENCE         MELSKDIMVHFKQHMQNQSDSGPID-LTVNILTMGYWPTYTP-
MEVHLTP 545
3DQV_C|PDBID|CHAIN|SEQUENCE
IKVSEDLNQAFKEMHKNNKLALPADSVNIKILNAGAWSRSSEKVFVSLPT 151
                                :::*:*:   **:  :*:. : * * :.::**. * *.  :  : *
*..

2HYE_C|PDBID|CHAIN|SEQUENCE
EMIKLQEVFKAFYLGKHSGRKLQWQTTLGHAVLKAEFKEGKKEFQVSLFQ 595
3DQV_C|PDBID|CHAIN|SEQUENCE
ELEDLIPEVEEFYKKNHSGRKLHWHHLMSNGIITFKNEVGQYDLEVTTFQ 201
                                *: .*    .: **   :******:*:   :.:.::. : : *:
:::*: **

2HYE_C|PDBID|CHAIN|SEQUENCE        TLVLLMFNEG--DGFSFEEIKMATGIEDSELRRTLQSLACG---
KARVLI 640
```

```
3DQV_C|PDBID|CHAIN|SEQUENCE
LAVLFAWNQRPREKISFENLKLATELPDAELRRTLWSLVAFPKLKRQVLL 251
                                  **: :*:   : :***::*:** : *:****** **..    *
:**:

2HYE_C|PDBID|CHAIN|SEQUENCE                         KSPKG---KEVEDGDKFIFNGEF-----
KHKLFRIKINQIQMKETVEEQV 682
3DQV_C|PDBID|CHAIN|SEQUENCE
YEPQVNSPKDFTEGTLFSVNQEFSLIKNAKVQKRGKINLIGRLQLTTERM 301
                                 .*:    *:. :*  * .* **      :   * *** *   : .
*::

2HYE_C|PDBID|CHAIN|SEQUENCE                                                STTER--
VFQDRQYQIDAAIVRIMKMRKTLGHNLLVSELYNQLKFPVKPG 730
3DQV_C|PDBID|CHAIN|SEQUENCE
REEENEGIVQLRILRTQEAIIQIMKMRKKISNAQLQTELVEILKNMFLPQ 351
                                   *.  :.* *  : : **::******.:.:  * :** : **
. *

2HYE_C|PDBID|CHAIN|SEQUENCE      D--LKKRIESLIDRDYMERDKDNPNQYHYVA 759
3DQV_C|PDBID|CHAIN|SEQUENCE      KKMIKEQIEWLIEHKYIRRDESDINTFIYMA 382
                                 .  :*::** **::.*:.**:.: * : *:*
```

REFERENCES

1. Ciechanover, A., The Ubiquitin-Proteasome Pathway: on Protein Death and Cell Life, *The EMBO Journal*, Vol. 17, pp. 7151-7160, Dec 1998.

2. Ciechanover, A. and A. L. Schwartz, The Ubiquitin-Proteasome Pathway: the Complexity and Myriad Functions of Proteins Death, *Proceedings of the National Academy of Sciences of the United States of America*, Vol. 95, pp. 2727-2730, Mar 1998.

3. Hershko, A., The Ubiquitin System for Protein Degradation and Some of Its Roles in the Control of the Cell-Division Cycle (Nobel Lecture), *Angewandte Chemie*, Vol. 44, pp. 5932-5943, Sep 2005.

4. Zimmerman, E. S., B. A. Schulman, and N. Zheng, Structural Assembly of Cullin-RING Ubiquitin Ligase Complexes, *Current Opinion in Structural Biology*, Vol. 20, pp. 714-21, Dec 2010.

5. Hershko, A. and A. Ciechanover, The Ubiquitin System, *Annual Review of Biochemistry*, Vol. 67, pp. 425-479, 1998.

6. Glickman, M. H. and A. Ciechanover, The Ubiquitin-Proteasome Proteolytic Pathway: Destruction for the Sake of Construction, *Physiological Reviews*, Vol. 82, pp. 373-428, Apr 2002.

7. Capili, A. D. and C. D. Lima, Taking it Step by Step: Mechanistic Insights from Structural Studies of Ubiquitin/Ubiquitin-Like Protein Modification Pathways, *Current Opinion in Structural Biology*, Vol. 17, pp. 726-735, Dec 2007.

8. Deshaies, R. J. and C. A. Joazeiro, RING Domain E3 Ubiquitin Ligases, *Annual Review of Biochemistry*, Vol. 78, pp. 399-434, 2009.

9. Petroski, M. D. and R. J. Deshaies, Function and Regulation of Cullin-RING Ubiquitin Ligases, *Nature Reviews - Molecular cell biology*, Vol. 6, pp. 9-20, Jan 2005.

10. Hershko, A., The Ubiquitin System for Protein Degradation and Some of Its Roles in the Control of the Cell Division Cycle, *Cell Death and Differentiation*, Vol. 12, pp. 1191-1197, Sep 2005.

11. Duncan, K., G. Schafer, A. Vava, M. I. Parker, and L. F. Zerbini, Targeting Neddylation in Cancer Therapy, *Future Oncology*, Vol. 8, pp. 1461-1470, Nov 2012.

12. Soucy, T. A., L. R. Dick, P. G. Smith, M. A. Milhollen, and J. E. Brownell, The NEDD8 Conjugation Pathway and Its Relevance in Cancer Biology and Therapy, *Genes & Cancer*, Vol. 1, pp. 708-716, Jul 2010.

13. Tanaka, T., T. Nakatani, and T. Kamitani, Inhibition of NEDD8-Conjugation Pathway by Novel Molecules: Potential Approaches to Anticancer Therapy, *Molecular Oncology*, Vol. 6, pp. 267-275, Jun 2012.

14. Liu, J. and R. Nussinov, The Role of Allostery in the Ubiquitin-Proteasome System, *Critical Reviews in Biochemistry and Molecular Biology*, Vol. 48, pp. 89-97, Apr 2013.

15. Cui, Q. and M. Karplus, Allostery and Cooperativity Revisited, *Protein Science: a Publication of the Protein Society*, Vol. 17, pp. 1295-307, Aug 2008.

16. Ma, B., C. J. Tsai, T. Haliloglu, and R. Nussinov, Dynamic Allostery: Linkers are Not Merely Flexible, *Structure*, Vol. 19, pp. 907-17, Jul 2011.

17. Rabut, G. and M. Peter, Function and Regulation of Protein Neddylation, *EMBO Reports*, Vol. 9, pp. 969-976, Oct 2008.

18. Zhao, Y., M. A. Morgan, and Y. Sun, Targeting Neddylation Pathways to Inactivate Cullin-RING Ligases for Anticancer Therapy, *Antioxidants & Redox Signaling*, Feb 2014.

19. Lydeard, J. R., B. A. Schulman, and J. W. Harper, Building and Remodelling Cullin-RING E3 Ubiquitin Ligases, *EMBO Reports*, Vol. 14, pp. 1050-1061, Dec 2013.

20. Duda, D. M., L. A. Borg, D. C. Scott, H. W. Hunt, M. Hammel, and B. A. Schulman, Structural Insights into NEDD8 Activation of Cullin-RING Ligases: Conformational Control of Conjugation, *Cell*, Vol. 134, pp. 995-1006, Sep 2008.

21. Luo, Z., Y. Pan, L. S. Jeong, J. Liu, and Jia, L., Inactivation of the Cullin (CUL)-RING E3 Ligase by the NEDD8-Activating Enzyme Inhibitor MLN4924 Triggers Protective Autophagy in Cancer Cells, *Autophagy*, Vol. 8, pp. 1677-1679, Nov 2012.

22. Li, L., M. Wang, G. Yu, P. Chen, H. Li, D. Wei, J. Zhu, L. Xie, H. Jia, J. Shi, C. Li, W. Yao, Y. Wang, Q. Gao, L. S. Jeong, H. W. Lee, J. Yu, F. Hu, J. Mei, P. Wang, Y. Chu, H. Qi, M. Yang, Z. Dong, Y. Sun, R. M. Hoffman, and L. Jia, Overactivated Neddylation Pathway as a Therapeutic Target in Lung Cancer, *Journal of the National Cancer Institute*, Vol. 106, Jun 2014.

23. Yao, W. T., J. F. Wu, G. Y. Yu, R. Wang, K. Wang, L. H. Li, P. Chen, Y. N. Jiang, H. Cheng, H. W. Lee, J. Yu, H. Qi, X. J. Yu, P. Wang, Y. W. Chu, M. Yang, Z. C. Hua, H. Q. Ying, R. M. Hoffman, L. S. Jeong, and L. J. Jia, Suppression of Tumor Angiogenesis by Targeting the Protein Neddylation Pathway, *Cell Death & Disease*, Vol. 5, pp. 1059, 2014.

24. Chen, D., M. Frezza, S. Schmitt, J. Kanwar, and Q. P. Dou, Bortezomib as the First Proteasome Inhibitor Anticancer Drug: Current Status and Future Perspectives, *Current Cancer Drug Targets*, Vol. 11, pp. 239-53, Mar 2011.

25. Goldstein, G., M. Scheid, U. Hammerling, D. H. Schlesinger, H. D. Niall, and E. A. Boyse, Isolation of a Polypeptide that Has Lymphocyte-Differentiating Properties and is Probably Represented Universally in Living Cells, *Proceedings of the National Academy of Sciences of the United States of America*, Vol. 72, pp. 11-15, Jan 1975.

26. Neefjes, J., T. A. Groothuis, and N. P. Dantuma, The 2004 Nobel Prize in Chemistry for the Discovery of Ubiquitin-Mediated Protein Degradation, *Nederlands Tijdschrift Voor Geneeskunde*, Vol. 148, pp. 2579-2582, Dec 2004.

27. Kimura, Y. and K. Tanaka, Regulatory Mechanisms Involved in the Control of Ubiquitin Homeostasis, *Journal of Biochemistry*, Vol. 147, pp. 793-798, Jun 2010.

28. Chen, Z. J. and L. J. Sun, Nonproteolytic Functions of Ubiquitin in Cell Signaling, *Molecular Cell,* Vol. 33, pp. 275-286, Feb 2009.

29. Skaug, B., X. Jiang, and Z. J. Chen, The Role of Ubiquitin in NF-KappaB Regulatory Pathways, *Annual Review of Biochemistry,* Vol. 78, pp. 769-796, 2009.

30. Bennett, E. J. and J. W. Harper, DNA Damage: Ubiquitin Marks the Spot, *Nature Structural & Molecular Biology,* Vol. 15, pp. 20-22, Jan 2008.

31. Ulrich, H. D. and H. Walden, Ubiquitin Signalling in DNA Replication and Repair, *Nature Reviews. Molecular Cell Biology,* Vol. 11, pp. 479-489, Jul 2010.

32. Acconcia, F., S. Sigismund, and S. Polo, Ubiquitin in Trafficking: The Network at Work, *Experimental Cell Research,* Vol. 315, pp. 1610-1618, May 2009.

33. Kamitani, T., K. Kito, H. P. Nguyen, and E. T. Yeh, Characterization of NEDD8, a Developmentally Down-Regulated Ubiquitin-Like Protein, *The Journal of Biological Chemistry,* Vol. 272, pp. 28557-28562, Nov 1997.

34. Kumar, S., Y. Tomooka, and M. Noda, Identification of a Set of Genes with Developmentally Down-Regulated Expression in the Mouse Brain, *Biochemical and Biophysical Research Communications,* Vol. 185, pp. 1155-11561, Jun 1992.

35. Ciechanover, A., Intracellular Protein Degradation: From a Vague Idea Thru the Lysosome and The Ubiquitin-Proteasome System and Onto Human Diseases and Drug Targeting, *Cell Death and Differentiation,* Vol. 12, pp. 1178-1190, Sep 2005.

36. Haas, A. L., J. V. Warms, A. Hershko, and I. A. Rose, Ubiquitin-Activating Enzyme Mechanism and Role in Protein-Ubiquitin Conjugation, *The Journal of Biological Chemistry,* Vol. 257, pp. 2543-2548, Mar 1982.

37. Ciechanover, A., S. Elias, H. Heller, and A. Hershko, Covalent Affinity Purification of Ubiquitin-Activating Enzyme, *The Journal of Biological Chemistry,* Vol. 257, pp. 2537-2542, Mar 1982.

38. Groettrup, M., C. Pelzer, G. Schmidtke, and K. Hofmann, Activating the Ubiquitin Family: UBA6 Challenges the Field, *Trends in Biochemical Sciences,* Vol. 33, pp. 230-237, May 2008.

39. Myung, J., K. B. Kim, and C. M. Crews, The Ubiquitin-Proteasome Pathway and Proteasome Inhibitors, *Medicinal Research Reviews,* Vol. 21, pp. 245-273, Jul 2001.

40. Wei, N., G. Serino, and X. W. Deng, The COP9 Signalosome: More Than a Protease, *Trends in Biochemical Sciences,* Vol. 33, pp. 592-600, Dec 2008.

41. Chan, Y., J. Yoon, J. T. Wu, H. J. Kim, K. T. Pan, J. Yim, and C. T. Chien, DEN1 Deneddylates Non-Cullin Proteins in Vivo, *Journal of Cell Science,* Vol. 121, pp. 3218-3223, Oct 2008.

42. Duda, D. M., D. C. Scott, M. F. Calabrese, E. S. Zimmerman, N. Zheng, and B. A. Schulman, Structural Regulation of Cullin-RING Ubiquitin Ligase Complexes, *Current Opinion in Structural Biology,* Vol. 21, pp. 257-264, Apr 2011.

43. Bosu, D. R. and E. T. Kipreos, Cullin-RING Ubiquitin Ligases: Global Regulation and Activation Cycles, *Cell Division,* Vol. 3, pp. 7, 2008.

44. Kar, G., O. Keskin, R. Nussinov, and A. Gursoy, Human Proteome-Scale Structural Modeling of E2-E3 Interactions Exploiting Interface Motifs, *Journal of Proteome Research,* Vol. 11, pp. 1196-1207, Feb 2012.

45. Sarikas, A., T. Hartmann, and Z. Q. Pan, The Cullin Protein Family, *Genome Biology,* Vol. 12, pp. 220, 2011.

46. Liu, J. and R. Nussinov, Rbx1 Flexible Linker Facilitates Cullin-RING Ligase Function before Neddylation and after Deneddylation, *Biophysical Journal,* Vol. 99, pp. 736-744, Aug 2010.

47. Watson, I. R., M. S. Irwin, and M. Ohh, NEDD8 Pathways in Cancer, Sine Quibus Non, *Cancer Cell,* Vol. 19, pp. 168-176, Feb 2011.

48. Saifee, N. H. and N. Zheng, A Ubiquitin-Like Protein Unleashes Ubiquitin Ligases, *Cell*, Vol. 135, pp. 209-211, Oct 2008.

49. Melzner, I., A. J. Bucur, S. Bruderlein, K. Dorsch, C. Hasel, T. F. Barth, F. Leithauser, and P. Moller, Biallelic Mutation of SOCS-1 Impairs JAK2 Degradation and Sustains Phospho-JAK2 Action in the MedB-1 Mediastinal Lymphoma Line, *Blood*, Vol. 105, pp. 2535-2542, Mar 2005.

50. He, B., L. You, K. Uematsu, K. Zang, Z. Xu, A. Y. Lee, J. F. Costello, F. McCormick, and D. M. Jablons, SOCS-3 is Frequently Silenced by Hypermethylation and Suppresses Cell Growth in Human Lung Cancer, *Proceedings of the National Academy of Sciences of the United States of America*, Vol. 100, pp. 14133-14138, Nov 2003.

51. Querido, E., M. R. Morrison, H. Chu-Pham-Dang, S. W. Thirlwell, D. Boivin, and P. E. Branton, Identification of Three Functions of the Adenovirus E4orf6 Protein that Mediate p53 Degradation by the E4orf6-E1B55K Complex, *Journal of Virology*, Vol. 75, pp. 699-709, Jan 2001.

52. Cai, Q. L., J. S. Knight, S. C. Verma, P. Zald, and E. S. Robertson, EC5S Ubiquitin Complex is Recruited by KSHV Latent Antigen LANA for Degradation of the VHL and p53 Tumor Suppressors," *Plos Pathogens*, Vol. 2, pp. 116, Oct 2006.

53. Ehrlich, E. S., T. Wang, K. Luo, Z. Xiao, A. M. Niewiadomska, T. Martinez, W. Xu, L. Neckers, and X. F. Yu, Regulation of Hsp90 Client Proteins by a Cullin5-RING E3 Ubiquitin Ligase, *Proceedings of the National Academy of Sciences of the United States of America*, Vol. 106, pp. 20330-20335, Dec 2009.

54. Stanley, D. J., K. Bartholomeeusen, D. C. Crosby, D. Y. Kim, E. Kwon, L. Yen, N. C. Cartozo, M. Li, S. Jager, J. Mason-Herr, F. Hayashi, S. Yokoyama, N. J. Krogan, R. S. Harris, B. M. Peterlin, and J. D. Gross, Inhibition of a NEDD8 Cascade Restores Restriction of HIV by APOBEC3G, *PLoS Pathogens*, Vol. 8, pp. 1003085, Dec 2012.

55. Liu, J. and R. Nussinov, The Mechanism of Ubiquitination in the Cullin-RING E3 Ligase Machinery: Conformational Control of Substrate Orientation, *PLoS Computational Biology*, Vol. 5, pp. 1000527, Oct 2009.

56. Liu, J. and R. Nussinov, Flexible Cullins in Cullin-RING E3 Ligases Allosterically Regulate Ubiquitination, *The Journal of Biological Chemistry*, Vol. 286, pp. 40934-40942, Nov 2011.

57. Richardson, P. G., P. Sonneveld, M. W. Schuster, D. Irwin, E. A. Stadtmauer, T. Facon, J. L. Harousseau, D. Ben-Yehuda, S. Lonial, H. Goldschmidt, D. Reece, J. F. San-Miguel, J. Blade, M. Boccadoro, J. Cavenagh, W. S. Dalton, A. L. Boral, D. L. Esseltine, J. B. Porter, D. Schenkein, and K. C. Anderson, Bortezomib or High-Dose Dexamethasone for Relapsed Multiple Myeloma, *The New England Journal of Medicine*, Vol. 352, pp. 2487-2498, Jun 2005.

58. San Miguel, J. F., R. Schlag, N. K. Khuageva, M. A. Dimopoulos, O. Shpilberg, M. Kropff, I. Spicka, M. T. Petrucci, A. Palumbo, O. S. Samoilova, A. Dmoszynska, K. M. Abdulkadyrov, R. Schots, B. Jiang, M. V. Mateos, K. C. Anderson, D. L. Esseltine, K. Liu, A. Cakana, H. Van de Velde, and P. G. Richardson, Bortezomib Plus Melphalan and Prednisone for Initial Treatment of Multiple Myeloma, *The New England Journal of Medicine*, Vol. 359, pp. 906-917, Aug 2008.

59. Nawrocki, S. T., P. Griffin, K. R. Kelly, and J. S. Carew, MLN4924: a Novel First-in-Class Inhibitor of NEDD8-Activating Enzyme for Cancer Therapy, *Expert Opinion on Investigational Drugs*, Vol. 21, pp. 1563-73, Oct 2012.

60. Deshaies, R. J., E. D. Emberley, and A. Saha, Control of Cullin-Ring Ubiquitin Ligase Activity by Nedd8, *Sub-Cellular Biochemistry*, Vol. 54, pp. 41-56, 2010.

61. Karplus, M. and G. A. Petsko, Molecular-Dynamics Simulations in Biology, *Nature*, Vol. 347, pp. 631-639, Oct 1990.

62. Brooks, B. R., R. E. Bruccoleri, B. D. Olafson, D. J. States, S. Swaminathan, and M. Karplus, Charmm- a Program for Macromolecular Energy, Minimization, and

Dynamics Calculations, *Journal of Computational Chemistry,* Vol. 4, pp. 187-217, 1983.

63. Brooks, B. R., C. L. Brooks, A. D. Mackerell, L. Nilsson, R. J. Petrella, B. Roux, Y. Won, G. Archontis, C. Bartels, S. Boresch, A. Caflisch, L. Caves, Q. Cui, A. R. Dinner, M. Feig, S. Fischer, J. Gao, M. Hodoscek, W. Im, K. Kuczera, T. Lazaridis, J. Ma, V. Ovchinnikov, E. Paci, R. W. Pastor, C. B. Post, J. Z. Pu, M. Schaefer, B. Tidor, R. M. Venable, H. L. Woodcock, X. Wu, W. Yang, D. M. York, and M. Karplus, CHARMM: The Biomolecular Simulation Program, *Journal of Computational Chemistry,* Vol. 30, pp. 1545-1614, Jul 2009.

64. Haliloglu, T., I. Bahar, and B. Erman, Gaussian Dynamics of Folded Proteins, *Physical Review Letters,* Vol. 79, pp. 3090-3093, Oct 1997.

65. Yang, L. W., A. J. Rader, X. Liu, C. J. Jursa, S. C. Chen, H. A. Karimi, and I. Bahar, oGNM: Online Computation of Structural Dynamics Using the Gaussian Network Model, *Nucleic Acids Research,* Vol. 34, pp. 24-31, Jul 2006.

66. Meller, J., Molecular Dynamics, *Encyclopedia of Life Sciences,* 2001.

67. Allen, M. P., Introduction to Molecular Dynamics Simulation, Vol. 23, ed: *Computational Soft Matter: From Synthetic Polymers to Proteins,* pp. 1-28, 2004.

68. Field, M. J., P. A. Bash, and M. Karplus, A Combined Quantum-Mechanical and Molecular Mechanical Potential for Molecular-Dynamics Simulations, *Journal of Computational Chemistry,* Vol. 11, pp. 700-733, Jul 1990.

69. Leach, A. R., *Molecular Modelling Principles and Applications,* second ed. Pearson, 2001.

70. Eswar, N., B. Webb, M. A. Marti-Renom, M. S. Madhusudhan, D. Eramian, M. Y. Shen, U. Pieper, and A. Sali, Comparative Protein Structure Modeling Using Modeller, *Current Protocols in Bioinformatics,* Vol. Chapter 5, Oct 2006.

71. Phillips, J. C., R. Braun, W. Wang, J. Gumbart, E. Tajkhorshid, E. Villa, C. Chipot, R. D. Skeel, L. Kale, and K. Schulten, Scalable Molecular Dynamics with NAMD, *Journal of Computational Chemistry*, Vol. 26, pp. 1781-1802, Dec 2005.

72. Levy, R. M., M. Karplus, and J. A. Mccammon, Diffusive Langevin Dynamics of Model Alkanes, *Chemical Physics Letters*, Vol. 65, pp. 4-11, 1979.

73. Ryckaert, J. P., G. Ciccotti, and H. J. C. Berendsen, Numerical Integration of the Cartesian Equations of Motion of a System with Constraints: Molecular Dynamics of n-alkanes, Journal of Comput Phys, Vol. 23, pp. 327-341, 1977.

74. Jorgensen, W. L., J. Chandrasekhar, J. D. Madura, R. W. Impey, and M. L. Klein, Comparison of Simple Potential Functions for Simulating Liquid Water, *Journal of Chemical Physics*, Vol. 79, pp. 926-935, 1983.

75. Darden, T., D. York, and L. Pedersen, Particle Mesh Ewald - an N.Log(N) Method for Ewald Sums in Large Systems, *Journal of Chemical Physics*, Vol. 98, pp. 10089-10092, Jun 1993.

76. Humphrey, W., A. Dalke, and K. Schulten, VMD: Visual Molecular Dynamics, *Journal of Molecular Graphics & Modelling*, Vol. 14, pp. 33-38, Feb 1996.

77. Wang, J., W. Wang, P. A. Kollman, and D. A. Case, Automatic Atom Type and Bond Type Perception in Molecular Mechanical Calculations, *Journal of Molecular Graphics & Modelling*, Vol. 25, pp. 247-260, Oct 2006.

78. Jolliffe, I. T., *Principal Component Analysis*, 2002.

79. Feig, M., J. Karanicolas, and C. L. Brooks, 3rd, MMTSB Tool Set: Enhanced Sampling and Multiscale Modeling Methods for Applications in Structural Biology, *Journal of Molecular Graphics & Modelling*, Vol. 22, pp. 377-395, May 2004.

80. Karpen, M. E., D. J. Tobias, and C. L. Brooks, Statistical Clustering Techniques for the Analysis of Long Molecular Dynamics Trajectories: Analysis of 2.2-Ns Trajectories of YPGDV, *Biochemistry*, Vol. 32, pp. 412-420, Jan 1993.

81. Torda, A. E. and W. F. Vangunsteren, Algorithms for Clustering Molecular-Dynamics Configurations, *Journal of Computational Chemistry*, Vol. 15, pp. 1331-1340, Dec 1994.

82. Best, C. and H. C. Hege, Visualizing and Identifying Conformational Ensembles in Molecular Dynamics Trajectories, *Computing in Science & Engineering*, Vol. 4, pp. 68-75, May-Jun 2002.

83. Bahar, I. and A. J. Rader, Coarse-Grained Normal Mode Analysis in Structural Biology, *Current Opinion in Structural Biology*, Vol. 15, pp. 586-592, Oct 2005.

84. Bahar, I., B. Erman, T. Haliloglu, and R. L. Jernigan, Efficient Characterization of Collective Motions and Interresidue Correlations in Proteins by Low-Resolution Simulations, *Biochemistry*, Vol. 36, pp. 13512-13523, Nov 1997.

85. Flory, P. J., Statistical Thermodynamics of Random Networks, *Proceedings of the Royal Society of London Series a-Mathematical Physical and Engineering Sciences*, Vol. 351, pp. 351-380, 1976.

86. Haliloglu, T., E. Seyrek, and B. Erman, Prediction of Binding Sites in Receptor-Ligand Complexes with the Gaussian Network Model, *Physical Review Letters*, Vol. 100, p. 228102, Jun 2008.

87. Haliloglu, T. and B. Erman, Analysis of Correlations Between Energy and Residue Fluctuations in Native Proteins and Determination of Specific Sites for Binding, *Physical Review Letters*, Vol. 102, Feb 2009.

88. Marques, O., BLZPACK: Description and User's Guide, 1995.

89. Wriggers, W. and K. Schulten, Protein Domain Movements: Detection of Rigid Domains and Visualization of Hinges in Comparisons of Atomic Coordinates, *Proteins-Structure Function and Genetics*, Vol. 29, pp. 1-14, Sep 1997.

90. Calabrese, M. F., D. C. Scott, D. M. Duda, C. R. Grace, I. Kurinov, R. W. Kriwacki, and B. A. Schulman, A RING E3-Substrate Complex Poised for Ubiquitin-Like

Protein Transfer: Structural Insights into Cullin-RING Ligases, *Nature Structural & Molecular Biology,* Vol. 18, pp. 947-949, Aug 2011.

91. Angers, S., T. Li, X. Yi, M. J. MacCoss, R. T. Moon, and N. Zheng, Molecular Architecture and Assembly of the DDB1-CUL4A Ubiquitin Ligase Machinery, *Nature,* Vol. 443, pp. 590-593, Oct 2006.